

University of Kentucky

UKnowledge

Theses and Dissertations--Mechanical
Engineering

Mechanical Engineering


2023

A computational fluid dynamic analysis of oxyacetylene combustion flow for use in material response boundary conditions

Craig Meade

University of Kentucky, craig.meade@outlook.com

Author ORCID Identifier:

 <https://orcid.org/0000-0002-1061-5522>

Digital Object Identifier: <https://doi.org/10.13023/etd.2023.491>

[Right click to open a feedback form in a new tab to let us know how this document benefits you.](#)

Recommended Citation

Meade, Craig, "A computational fluid dynamic analysis of oxyacetylene combustion flow for use in material response boundary conditions" (2023). *Theses and Dissertations--Mechanical Engineering*. 217. https://uknowledge.uky.edu/me_etds/217

This Master's Thesis is brought to you for free and open access by the Mechanical Engineering at UKnowledge. It has been accepted for inclusion in Theses and Dissertations--Mechanical Engineering by an authorized administrator of UKnowledge. For more information, please contact UKnowledge@lsv.uky.edu.

STUDENT AGREEMENT:

I represent that my thesis or dissertation and abstract are my original work. Proper attribution has been given to all outside sources. I understand that I am solely responsible for obtaining any needed copyright permissions. I have obtained needed written permission statement(s) from the owner(s) of each third-party copyrighted matter to be included in my work, allowing electronic distribution (if such use is not permitted by the fair use doctrine) which will be submitted to UKnowledge as Additional File.

I hereby grant to The University of Kentucky and its agents the irrevocable, non-exclusive, and royalty-free license to archive and make accessible my work in whole or in part in all forms of media, now or hereafter known. I agree that the document mentioned above may be made available immediately for worldwide access unless an embargo applies.

I retain all other ownership rights to the copyright of my work. I also retain the right to use in future works (such as articles or books) all or part of my work. I understand that I am free to register the copyright to my work.

REVIEW, APPROVAL AND ACCEPTANCE

The document mentioned above has been reviewed and accepted by the student's advisor, on behalf of the advisory committee, and by the Director of Graduate Studies (DGS), on behalf of the program; we verify that this is the final, approved version of the student's thesis including all changes required by the advisory committee. The undersigned agree to abide by the statements above.

Craig Meade, Student

Dr. Alexandre Martin, Major Professor

Dr. Johnathan Wenk, Director of Graduate Studies

A computational fluid dynamic analysis of oxyacetylene combustion flow for use in
material response boundary conditions

THESIS

A thesis submitted in partial
fulfillment of the requirements for
the degree of Master of Science in
the College of Engineering at the
University of Kentucky

By

Craig Samuel Meade

Louisville, Kentucky

Director: Dr. Alexandre Martin, Professor of Mechanical and Aerospace Engineering

Lexington, Kentucky

2023

Copyright© Craig Samuel Meade 2023

ABSTRACT OF THESIS

A computational fluid dynamic analysis of oxyacetylene combustion flow for use in material response boundary conditions

Oxyacetylene torches are used in the aerospace industry and research to test thermal protection system materials (TPS) due to their high flame temperatures and high heat flux capabilities. The purpose of this work is to determine a combustion model to accurately simulate the high temperature flow of an oxyacetylene torch. The flow conditions around a sample material can then be used as boundary conditions when modeling TPS material response. Two separate combustion models with equilibrium chemistry were investigated using ANSYS FluentTM; the Eddy-Dissipation Model, and the Partially Premixed model. The results of this study are compared to existing experiments for validation.

KEYWORDS: combustion, oxyacetylene, aerothermodynamics, material response, thermal protection systems

Craig Samuel Meade

December 16, 2023

A computational fluid dynamic analysis of oxyacetylene combustion flow for use in
material response boundary conditions

By

Craig Samuel Meade

Dr. Alexandre Martin

Director of Thesis

Dr. Jonathan Wenk

Director of Graduate Studies

December 16, 2023

Date

This work is dedicated to my wife, Megan Meade. I would not be writing this
today if not for you.

ACKNOWLEDGMENTS

I am incredibly grateful to Dr. Martin for allowing me to work with him, providing me with advice, and being a mentor to me. I am also very thankful for Dr. Poovathingal and Dr. Maddox, who agreed to be on my committee and who never minded my overzealous questions in class. I want to extend my sincerest gratitude to my wife, Megan for listening to my ramblings and supporting me through everything.

Thank you to my family and in-laws who have encouraged me through this process, especially my mother, Lisa Sosnin, who helped proofread this work. I also extend my gratitude to Alex Zibitsker for discussing KATS and material response and to everyone in the GSIL, CTFL, and Paducah labs for the friendship and encouragement you've shown me these last few years. I would also like to thank God for his guiding hand when I least deserved it.

TABLE OF CONTENTS

Acknowledgments	iii
List of Tables	vi
List of Figures	vii
Chapter 1 Introduction	1
1.1 Literature review	2
1.1.1 Flame impingement	2
1.1.2 Combustion models	3
1.1.3 Experiments and CFD	3
1.1.4 Material response	4
Chapter 2 Governing equations	6
2.1 Navier-Stokes equations	6
2.2 Species transport	7
2.3 Reynolds-Averaged Navier-Stokes (RANS)	8
2.3.1 Turbulence	9
2.4 Combustion models	11
2.4.1 Chemical equilibrium assumption	12
2.4.2 Eddy-Dissipation model	13
2.4.3 Partially Premix model	15
2.5 Radiation	18
2.6 Discretization	19
Chapter 3 Methodology	20
3.1 Overview	20

3.2	Experiment discussion	22
3.3	Geometry creation	25
3.4	Mesh and grid independence	25
3.5	Solver	29
3.5.1	Initial conditions	30
3.5.2	Boundary conditions	31
3.5.3	Initialization and calculation	33
Chapter 4	Results and discussion	34
4.1	Marra experiment	34
4.2	Miller-Oana experiment	42
Chapter 5	Conclusions and future work	63
5.1	Future work	64
Appendices	65
Appendix A	Partial Pressure custom function	66
Appendix B	Automatic initialization commands (Cold Flow)	67
Appendix C	Automatic initialization commands (Combustion)	68
Appendix D	Custom Ablative Material	69
Bibliography	70
Vita	75

LIST OF TABLES

3.1	Mesh cell count	26
3.2	Miller-Oana Fuel Inlet Conditions	32
3.3	Marra Fuel Initial Conditions	32
3.4	Boundary condition summary	33
4.1	Gauge and ablative sample result comparison with Marra et al.[1] and Fortner [2]	38
4.2	Computational requirement comparison of Marra et al. [1] and this study for the gauge study	39

LIST OF FIGURES

2.1	Transient and time average comparison	9
2.2	A diagram of Partially Premix variables within a flame	17
2.3	Infinite radiating beams converted to Discrete Ordinates sectors	19
3.1	Parametric study flowchart	23
3.2	Torch tip comparison	24
3.3	Torch body example	24
3.4	3-D Geometry	25
3.5	Geometry	26
3.6	An overview of the entire fluid and solid domain mesh, (a) Overview of mesh, (b) sample mesh, (c) boundary layer	27
3.7	Boundary location and descriptions for the domain with a gauge.	28
3.8	Boundary location and descriptions	28
4.1	Eddy-Dissipation Method temperature contour plot spanning 4.5cm from nozzle tip to sample wall	35
4.2	Turbulent rate of reaction contour plot	36
4.3	Pressure profile along the copper gauge face	37
4.4	Wall y^+ along the face of the copper gauge case	37
4.5	Temperature contours of both fluid and solid domains using EDM Relation to Equilibrium (a) and Partially Premix combustion models (b)	40
4.6	Interior temperature contours of an Sigratherm [®] sample using EDM Re- lation to Equilibrium (a) and Partially Premix combustion models (b)	41
4.7	Ablative sample internal temperatures at various distances from the axis using EDM compared to Marra's CFD results	42

4.8	Temperature contour plot of the Eddy-Dissipation Model using direct-source terms in the species transport equation	43
4.9	Temperature contours at a distance of 5cm from nozzle tip to sample wall with 1.35 VFR for EDM (a) and Partially Premix combustion models(b)	44
4.10	Temperature contours at a sample distance of 11cm and a VFR of 1.35 for EDM (a) and Partially Premix combustion models (b)	45
4.11	EDM temperature contour of 1.5 VFR at 5cm from nozzle tip to sample wall	46
4.12	EDM temperature contour of 1.7 VFR at 5cm from nozzle tip to sample wall	46
4.13	EDM temperature contour of 1.35 VFR at 7cm from nozzle tip to sample wall	47
4.14	EDM temperature contour of 1.5 VFR at 7cm from nozzle tip to sample wall	47
4.15	EDM temperature contour of 1.7 VFR at 7cm from nozzle tip to sample wall	48
4.16	EDM temperature contour of 1.35 VFR at 9cm from nozzle tip to sample wall	48
4.17	EDM temperature contour of 1.5 VFR at 9cm from nozzle tip to sample wall	49
4.18	EDM temperature contour of 1.7 VFR at 9cm from nozzle tip to sample wall	49
4.19	EDM temperature contour of 1.5 VFR at 11cm from nozzle tip to sample wall	50
4.20	EDM temperature contour of 1.7 VFR at 11cm from nozzle tip to sample wall	50
4.21	The front face of a Gardon heat flux gauge with a small sensor area surrounded by cooled copper.	51

4.22	A comparison of heat flux values from 1.35,1.5, and 1.7 VFRs at distances from 5cm to 11cm.	52
4.23	Different VFR heat flux profiles on the face of the sample at distances of 5cm (a), 7cm (b), 9cm (c), and 11cm (d)	53
4.23	Different VFR heat flux profiles on the face of the sample at distances of 5cm (a), 7cm (b), 9cm (c), and 11cm (d)	54
4.24	Velocity comparison graph of non-reacting flow, Eddy-Dissipation Model, Partially Premixed Model, and Miller-Oana et al. where (A) cold reactants (B) pre-heat zone (C) secondary ignition	55
4.25	Temperature contour overlaid by velocity pathlines at 5cm from the torch tip to sample with a 1.35VFR using Partially Premixed model (b), and the Eddy-Dissipation model(a)	56
4.26	Partial pressure of O2 at distances along the flow axis	57
4.27	Static pressure profiles along the sample wall	58
4.28	Wall y+ profiles along the sample for EDM and Partially Premixed models at 5cm and 11 cm	58
4.29	Heat transfer coefficient (y+ based) along the sample wall	59
4.30	Nusselt values for the EDM with 1.35VFR at 11cm from the torch tip.	60
4.31	The boundary layer edge against velocity contour plot with a thickness of 0.4mm	61

Chapter 1 Introduction

Anything, including entry craft, rocket motors, and gas turbine blades, operating at extremely high speeds and temperatures, must be outfitted with a Thermal Protection System (TPS) to protect payloads and structures. The experimental methods used to test these materials are often costly and do not meet all operating criteria. For example, arc jet facilities lack the ability to produce operational shear and pressure, plasma and oxyacetylene torches do not operate at hypersonic speeds, solar towers create no flow shear, and supersonic wind and shock tunnels lack the ability to heat material properly. No single experimental test facility exists that can simulate such intense operational environments. Oxyacetylene torch facilities have limitations but offer an opportunity to test material at a high heat flux with a relatively cheap operating cost.

Direct hypersonic flights or numerical methods are the only ways all operational conditions can be applied to TPS material. The modern numerical method, Computational fluid dynamics (CFD), may be used to simulate flow, heat, and other conditions in a cost-effective manner. By using the aforementioned testing methods, data is obtained to validate the CFD models. This allows for proper design, manufacturing, and testing of exotic and costly materials in an efficient manner.

The purpose of this work is to establish an accurate and efficient CFD combustion model to obtain the flow conditions at the boundary layer of high-temperature combustion against a sample material. Upon acquiring proper flow conditions the material response of TPS materials may be evaluated in an uncoupled manner. Experimental results from Miller-Oana et al. [3] and Marra et al. [1] are used as validation of the CFD flow field. Two combustion models, the Eddy Dissipation and Partially Premixed models, are investigated using the assumption of chemical equilibrium and are discussed in greater detail in this work.

1.1 Literature review

This review briefly examines various aspects of solving for a combustion jet and the boundary layer conditions needed for material response.

1.1.1 Flame impingement

Flame impingement jets have long been used for industrial applications. For example: thermal spallation, where the flames impinge upon rock causing rapid thermal expansion and ejection of material; chemical vapor deposition (CVD), the manufacture of synthetic diamonds; industrial furnaces and coal beds; and testing of thermal protection systems (TPS). The latter is the application of interest for this study using oxyacetylene fuel. Oxyacetylene provides one of the highest flame temperatures at atmospheric pressure and is used in common applications such as welding. Glassman [4] reports a flame temperature for oxyacetylene at 3410K at an equivalence ratio of 1.7, and Strehlow [5] reports temperatures ranging from 3000K to 3500K for equivalence ratios of 0.4 to 1.8. These facts make the fuel one of the most readily available and reliable options to use in an experiment that simulates the high heating that occurs on devices that need TPS materials.

In the work by Zuckerman and Lior[6], non-combusting impinging jet heat transfer was investigated, providing good detail and validation for cold-flow studies, and the accuracy of various turbulence models to capture the heat transfer around an object. Zuckerman and Lior only mention flame impingement jets as a subset of impinging jets that typically have high turbulence in brief. The work by van der Meer [7] goes into more detail about this subset of jets, specifically focusing on the heat transfer of flame impinging jets. van der Meer describes the basic experimental procedure for a flame impingement on an isothermal flat plate; this is mirrored in the ASTM "Standard Test Method for Oxyacetylene Ablation Testing of Thermal Insulation Materials" [8]. The work by Baukal[9] provides a rich overview of flame impingement jets in general.

1.1.2 Combustion models

Combustion in general, is a complex phenomenon that is still experiencing ongoing research. Simplified methods have been created and investigated for non-premixed and premixed flames over the years. The Eddy-Dissipation model was created by Magnussen [10] and has gone through several iterations to increase accuracy. Oran and Bores [11] discuss numerical methods applied combustion modeling for various flows but specifically detail their use toward aerospace. Eddy-dissipation models have seen use in high-speed flows, specifically in supersonic [12] and scramjets [13] [14]. Oran and Bores' work describes reacting diffusion jets with high Damköhler numbers and premixed turbulent flames in detail.

Baukal[9] provides an overview and basic theory of CFD oxygen-enhanced combustion modeling using the Eddy-Dissipation model, Non-premixed, and Premixed combustion models used in this work. Baukal also discusses an overview of finite rate models like Flamelet models, as well as, statistical models like the PDF model; which are not used in this work.

The Partially Premixed model is the combination of the non-premixed and premixed models, i.e. the mixture fraction approach and progress variable approach, respectively. The mixture fraction approach was developed for single reaction mechanisms by Shvab and Zeldovich (translated NACA Technical Memorandum [15]), and later extended by Bilger [16], to use probability density functions for conditional moment closure using the mixture fractions and an assumed PDF shape [17]; similar in approach by ANSYS Fluent™[18]. The progress variable approach was described by Bray [19] in 1980 and later by Zimont et al.[20] [21] to describe the closure of the transport equation by use of the turbulent flame speed.

1.1.3 Experiments and CFD

All oxyacetylene torches are based on the ASTM standard mentioned earlier. The experimentalist modifies the variables such as distance to sample, mass flow, or equiv-

alence ratio to obtain the results they are investigating. Marra et al. [1] in 2011 executed both an experiment, and a CFD study with the Eddy-Dissipation Concept model and chemical kinetics on two samples - a copper Gardon gauge, and an ablative sample. In 2015 Miller-Oana[3] used an oxyacetylene torch to measure ablation rates of TPS materials which were validated using Fick's first law of diffusion.

Aydin et al. [22], like Marra, used both a CFD model for the flow of oxyacetylene and the heat transfer onto a sample as well as an experiment to validate against. The experiment used a heating torch tip, as opposed to the welding tips used by Miller-Oana and Marra, theoretically allowing higher heating on a sample. Aydin used Chemical Equilibrium Application (CEA) [23] to model the chemical equilibrium of a single-step reaction mechanism with eight products, to more accurately predict combustion with the Eddy-Dissipation Model. Then the Eddy-Dissipation Concept model was run to model the detailed reaction mechanisms from Westbrook and Dryer [24]. Fortner et al. [2] did similar work, but only investigated the Eddy-Dissipation model using direct-source chemistry terms with a single-step reaction mechanism.

1.1.4 Material response

The mid-1900s did not have the computing power that exists today; however, complex physical problems still existed for the new frontier. Before modern CFD, the heat flux on a device experiencing high temperatures had to be estimated through experimental and analytical means. The National Advisory Committee for Aeronautics published Technical Note 3706 [25] in 1956 which outlines previous work done in 1952 by Sibulkin [26] who had one of the first semi-analytical methods to determine heat transfer in stagnating flow. This method only considered forced convection but was later improved upon by Fay and Riddell [27] to incorporate enthalpy instead of temperature for heat transfer, and accounted for chemical dissociation at equilibrium. As Cooper [28] showed, the Fay and Riddell method can under-predict the heat flux compared to CFD; so though useful for the time, more work needed to be done. Baukal presents

an overview of the work done on the concept of heat transfer coefficient models and discusses them in detail [17][9]. The recent advancements in computing power have allowed complex problems, such as ablation, to be solved numerically through CFD. Three methods exist to solve to ablation problem: uncoupled (film coefficient method), partially-uncoupled, and fully coupled solvers. Bianchi [29] and Cooper [28] discuss the history of the film coefficient method and do an excellent job outlining the intersection of a CFD flow field and the material response for ablation problems. From these works, one may note that the heat flux, heat transfer coefficients, and pressures are needed from a CFD model as input into modern uncoupled material response solvers to solve ablation. Amar et al. [30] describe the use of an uncoupled analysis through the CHAR code, which uses convective heating and pressure solutions from the DPLR CFD code [31] as input. Amar et al. mention the harsh reality that although the codes are uncoupled, the real physics is not. The ablating surface ejects gas into the boundary layer, changing it's properties, therefore affecting the response of the ablative material. The coupling of the two solvers is where the future lies.

Chapter 2 Governing equations

The flow field is governed by the fundamental laws of physics and thermodynamics, i.e. conservation of mass, conservation of momentum, the conservation of energy (together known as the Navier Stokes equations), and an equation of state.

2.1 Navier-Stokes equations

The Law of Conservation of Mass, or Continuity, states that the net outflow of mass must equal the net inflow therefore conserving mass in a system. The 3-dimensional index notation of this law is stated in Eq. 2.1. Momentum is conserved through Newton's 2nd Law and shown in Eq. 2.2. The third equation and The First Law of Thermodynamics state that the net amount of energy input into a system must equal the net output of energy as shown in Eq. 2.3.

$$\frac{\partial \rho}{\partial t} + \frac{\partial(\rho u_i)}{\partial x_i} = 0 \quad (2.1)$$

$$\frac{\partial(\rho u_i)}{\partial t} + u_j \frac{\partial(\rho u_i)}{\partial x_j} = -\frac{\partial p}{\partial x_i} + \frac{\partial}{\partial x_j} \left(\mu \frac{\partial u_j}{\partial x_i} + \frac{\partial u_i}{\partial x_j} \right) \quad (2.2)$$

u_i = velocity vector

t = time

ρ = density

p = pressure

μ = dynamic viscosity

$$\frac{\partial(\rho E)}{\partial t} + u_j \frac{\partial(\rho E)}{\partial x_j} = -p \left(\frac{\partial u_j}{\partial x_j} \right) + \frac{\partial}{\partial x_j} \left(k \frac{\partial T}{\partial x_j} \right) + \Phi + S \quad (2.3)$$

where the dissipation function Φ is,

$$\Phi = \lambda \left(\frac{\partial u_j}{\partial x_j} \right)^2 + \mu \left(\frac{\partial u_j}{\partial x_i} + \frac{\partial u_j}{\partial x_i} \right) \frac{\partial u_j}{\partial x_i} \quad (2.4)$$

and the other variables shown are,

E = energy

T = temperature

k = thermal conductivity

The source term (S) is a link between the species transport equation and the energy equation through chemical reactions. The source term can be defined as,

$$S = \sum_j \frac{h_j^0}{M_j} R_j \quad (2.5)$$

where,

h_j^0 = enthalpy of formation of species j

M_j =

R_j = volumetric rate of creation of species j

When using the non-adiabatic non-premixed combustion model the heat of formation is included in enthalpy calculation, therefore reactions are not included in the energy source term[18].

2.2 Species transport

To accurately determine flame conditions the conservation equations for each species must also be solved. The species transport in Eq. 2.6 consists of advection, diffusion, and rate terms. During “cold flow” (no combustion) the reaction term drops out and the equation is solved for diffusion.

$$\frac{\partial(\rho Y_i)}{\partial t} + u_j \frac{\partial(\rho u_i Y_i)}{\partial x_j} = - \frac{\partial J_i}{\partial x_j} + R_i + S_i \quad (2.6)$$

Where,

Y_i = mass fraction of species

J_i = diffusion flux

R_i = reaction of species

S_i = the source term

2.3 Reynolds-Averaged Navier-Stokes (RANS)

Each set of equations in the previous section can be solved numerically for a discretized domain, called Direct Numerical Simulation or DNS. DNS combines all equations into a matrix, and then through several computations, arrives at a solution by solving the set equations directly for each time step and spatial area. DNS is therefore both time and computationally intensive even for a small domain.

To arrive at a numerically accurate solution without the need for high-performance computing this study used Reynolds-averaged Navier-Stokes (RANS). RANS averages the perturbations that physically occur in the flow over time. As an example, take the diffusion flame of a candle. Only the laminar outline of the flame itself is visible. If, however, we were able to take an image in a fraction of time, the turbulent mixing is shown. When the flow is averaged in time, the velocity u is no longer instantaneous but averaged. The pressure and velocity terms of the Navier-Stokes equations are decomposed into their respective average (\bar{u}) and fluctuating terms (u'), through Reynolds Decomposition.

$$u_i = \bar{u}_i + u'_i \qquad p = \bar{p} + p'$$

These terms are inserted back into our transport equations and integrated in time. As an example, Eq.2.7 is the averaged form of the momentum equation.

$$\rho \bar{u}_i \frac{\partial \bar{u}_j}{\partial x_j} = -\frac{\partial \bar{p}}{\partial x_j} + \frac{\partial}{\partial x_i} \left[\mu \left(\frac{\partial \bar{u}_i}{\partial x_j} + \frac{\partial \bar{u}_j}{\partial x_i} \right) - \overline{\rho u'_i u'_j} \right] \quad (2.7)$$

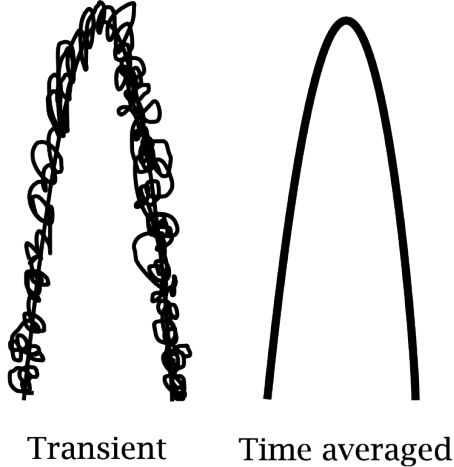


Figure 2.1: Transient and time average comparison

2.3.1 Turbulence

To simplify the equations further, the Boussinesq approximation is assumed and is the basis for $k-\omega$ and $k-\epsilon$ models. This approximation relates the Reynolds stresses Eq. 2.8 to the mean velocity gradients through turbulent eddy viscosity μ_t , Eq. 2.9, where k is the turbulent kinetic energy. This assumption also ignores small-scale vortices and uses an effective viscosity to transfer the momentum.

Again, looking at the Reynolds stress when applying the Boussinesq approximation,

$$\tau_{ij} = -\rho \overline{u'_i u'_j} \quad (2.8)$$

$$\tau_{ij} \approx 2\mu_t S_{ij} - \frac{2}{3}\rho k \delta_{ij} \quad (2.9)$$

The RANS equations must be closed with the use of other equations, and the new viscosity term solved for. The shear-stress transport (SST) $k-\omega$ SST model developed by Menter [32] was used in this work to solve for the turbulent eddy viscosity. This technique makes use of the $k-\epsilon$ model for the free-stream and $k-\omega$ model near the wall, by way of a blending function. Turbulent viscosity becomes a function of k and ω in the turbulent eddy viscosity term.

According to Menter [32], turbulent intensity (k) is given by the transport equation,

$$\rho \frac{\partial k}{\partial t} + \frac{\partial \rho u_j k}{\partial x_j} = \tau_{ij} \frac{\partial u_i}{\partial x_j} - \beta \rho k \omega + \frac{\partial}{\partial x_j} \left[(\mu + \sigma_k \mu_t) \frac{\partial k}{\partial x_j} \right]$$

and turbulent kinetic energy (ω) is given by,

$$\begin{aligned} \rho \frac{\partial \omega}{\partial t} + \frac{\partial \rho u_j \omega}{\partial x_j} &= \frac{\gamma}{\nu_t} \tau_{ij} \frac{\partial u_i}{\partial x_j} - \beta \rho \omega^2 \\ &+ \frac{\partial}{\partial x_j} \left[(\mu + \sigma_\omega \mu_t) \frac{\partial \omega}{\partial x_j} \right] + 2(1 - F_1) \frac{\rho \sigma_\omega}{\omega} \frac{\partial \omega}{\partial x_j} \partial \omega \partial x_j \end{aligned}$$

where,

ν_t = turbulent kinematic viscosity

μ = dynamic viscosity

$\mu_t = \frac{\rho a_i k}{\max(a_1 \omega, \Omega F_2)}$ = turbulent eddy viscosity

γ = coefficient

F_2 = blending function

a_1 = minimization function

and the left-hand term in Eq. 2.3.1 is the Production (P_k) term,

$$P_k = -\overline{\rho u'_i u'_j} \frac{\partial u_j}{\partial x_i} \quad (2.10)$$

Using the Boussinesq hypothesis mentioned earlier, the production term is transformed into,

$$P_k = -\mu_t S^2 \quad (2.11)$$

where the mean strain rate is composed of the strain rate tensor,

$$\begin{aligned} S &= \sqrt{2S_{ij}S_{ij}} \\ S_{ij} &= \frac{1}{2} \left(\frac{\partial u_i}{\partial x_j} + \frac{\partial u_j}{\partial x_i} \right) \end{aligned}$$

and the specific turbulent dissipation production is limited by the vorticity composed of the vorticity tensor,

$$\Omega = \sqrt{2\Omega_{ij}\Omega_{ij}}$$

$$\Omega_{ij} = \frac{1}{2} \left(\frac{\partial u_i}{\partial x_j} - \frac{\partial u_j}{\partial x_i} \right)$$

As summarized by Zuckerman and Lior [6], the $k - \omega$ SST model has moderate computation cost, good Nusselt, and heat transfer predictions for impingement jets, while ANSYS states it performs very well and without computational overhead [33]. Most turbulence models require the near-wall mesh to be refined to a wall $y^+ = 1$; however, the SST model has enhanced wall treatment. The enhanced wall treatment captures the high shear stress caused by significant pressure gradients from the impinging flow and allows accurate results to be obtained at greater wall y^+ . To accurately describe our boundary conditions and flow the turbulent intensity (I) and Reynolds number must be found and are defined below[33] as Eq.2.12

$$I = \frac{u'}{u_{avg}} \tag{2.12}$$

$$= 0.16(Re_{D_h})^{-1/8} \tag{2.13}$$

Where,

$$Re_{D_h} = \frac{\rho L_c u}{\mu} \tag{2.14}$$

These equations appear in the boundary conditions for the flow and also in chemistry assumptions, such as for Damköhler classification.

2.4 Combustion models

The flow from an oxyacetylene torch is a combination of diffusion combustion and premixed combustion. The oxygen and acetylene are thoroughly mixed in the welding torch mixing chamber, then ejected into a quiescent atmosphere and ignited. Atmospheric oxygen slowly advects into the flame of the combusting flow, similar to

non-premixed diffusion flames. There exist many methods for modeling this type of combustion; for example, the Eddy-Dissipation Model and Partially Premix Model. These two combustion models are the ones chosen to investigate in this work.

Damköhler number, along with other assumptions, play a large part in determining the type of combustion model used. As shown in Eq.2.15, the Damköhler number is the ratio of the flow time (τ_{flow}) and chemical time (τ_{chem}), thus approximating the combustion “speed”.

$$Da = \frac{\tau_{flow}}{\tau_{chem}} = \frac{l_0/v_{rms}}{\delta_L/S_L} \quad (2.15)$$

l_0 = integral length scale

v_{rms} = approximately the average velocity

δ_L = laminar flame thickness

S_L = laminar flame speed

2.4.1 Chemical equilibrium assumption

Chemical equilibrium occurs when the system has existed long enough for the species composition to be fixed and the forward and backward reaction rates are equal[34]. This study assumes chemistry is fast relative to the flow speed and the intermediate species composition is inconsequential; therefore, the reactions were relaxed to chemical equilibrium and the flow to its steady state. For reacting gas at chemical equilibrium, equations are algebraic and determined by the system pressure and temperature. Both combustion models described in this paper utilize the chemical equilibrium assumption; an assumption made in other combustion works by Aydin et al. [22], Ren et al. [35] [36], and Emami et al. [37].

2.4.2 Eddy-Dissipation model

The Eddy-Dissipation model (EDM) is based upon the work done by Magnussen and Hjertager [10] and assumes “fast” combustion chemistry relative to the flow speed, i.e large number Damköhler. The idea of “fast chemistry“ means that the reactions are mixing-limited so the rate of burning is controlled by the mixing rate where the complex chemical kinetic rates are ignored [17]; a fair assumption for oxyacetylene combustion.

With EDM the kinetic rates are irrelevant and the flow does not need an ignition source to combust only excessive turbulence. Premature ignition may occur in regions of the domain where there physically are none (such as the inside of a nozzle) due to the turbulence-chemistry interaction. The reaction variable of the species transport equation Eq. 2.6 is the lesser of Eqs. 2.16 and Eq. 2.17 when solving chemistry [33] and therefore the limiting reaction. This is the method of the “direct-source” chemistry solver in Fluent™.

$$R_{i,r} = (v''_{i,r} - v'_{i,r})M_{w,i}A\rho\frac{\epsilon}{k}min_R \left(\frac{Y_R}{v'_{R,r}M_{w,R}} \right) \quad (2.16)$$

$$R_{i,r} = (v''_{i,r} - v'_{i,r})M_{w,i}AB\rho\frac{\epsilon}{k} \left(\frac{\sum_P Y_P}{\sum_j^N v''_{j,r}M_{w,j}} \right) \quad (2.17)$$

where,

Y_R = mass fraction of reactant

Y_P = mass fraction of product

M_w = molecular weight of species

v' = stoichiometric coefficient for reactant

v'' = stoichiometric coefficient for product

N = number of species

A = empirical constant of 4.0

B = empirical constant of 0.5

This study makes the assumption of chemical equilibrium, where the species composition goes toward the equilibrium state. The reaction variable from the Species Transport equation is no longer the lesser of Eqs. 2.16 or 2.17 but instead becomes,

$$R_i = \rho \frac{Y_i^{eq} - Y_i}{\tau_{char}} \quad (2.18)$$

here the characteristic time scale is defined as,

$$\tau_{char} = \tau_{turb}$$

$$\tau_{turb} = \frac{k}{\epsilon A}$$

The reaction source term is independent of reaction mechanisms, simplifying the thermochemistry involved, and more accurately predicting the intermediate species like CO, O, and OH [18]. The "mixed is burnt" assumption is still valid as turbulence appears in the characteristic time equation. The use of the reaction variable as mass fraction has been shown to work reasonably well by itself as a CFD model for engine combustion and is considered expedient and practical [38].

2.4.3 Partially Premix model

Two types of combustion jets exist; non-premixed and premixed. Non-premixed flames model two distinct streams, an oxidizing stream, and the fuel stream, that only mix due to turbulence at the time of combustion; examples include gas lighters and diesel combustion. Premixed flames have a singular stream of fuel and oxidizer mixed on a molecular level before combustion occurs; examples of premixed jets are Bunsen burners and gasoline combustion.

An oxyacetylene torch is a combination of both where the oxygen and acetylene are mixed in the torch body (premix) but are expressed and mixed with air (non-premixed). Due to this combination, it was best to model the flow as both, e.g. the Partially Premix model.

The Partially Premix model is a combination of two other models, the Non-premixed and Premixed combustion models. Acetylene and oxygen are well mixed in a mixing chamber before ejection into the atmosphere; then air, acting as a secondary oxidizer, is entrained into the flame as combustion occurs. This model has the advantages and disadvantages of the previous two models because it is a combination of the others.

Non-premixed combustion models utilize conserved scalars and species concentration instead of individual species to solve the transport equations. This assumption simplifies the calculations by no longer solving for each species but for the mixture. The species conservation equation becomes similar to Eq. 2.6 except no reaction rate terms exist and therefore is “sourceless” [39].

$$\frac{\partial(\rho\bar{f})}{\partial t} + u_j \frac{\partial(\rho u_i \bar{f})}{\partial x_j} = \frac{\partial}{\partial x_i} \frac{\partial}{\partial x_i} \left(\frac{\mu_t}{\sigma_t} \bar{f} \right) + S_m \quad (2.19)$$

$$\frac{\partial(\rho\overline{f'^2})}{\partial t} + u_j \frac{\partial(\rho u_i \overline{f'^2})}{\partial x_j} = \frac{\partial}{\partial x_i} \frac{\partial}{\partial x_i} \left(\frac{\mu_t}{\sigma_t} \overline{f'^2} \right) + C_g \mu_t \left(\frac{\partial \bar{f}}{\partial x_i} \right)^2 - C_d \rho \frac{\epsilon}{k} \overline{f'^2} \quad (2.20)$$

Here the mixture fraction (f) is defined as,

$$f = \frac{Z_i - Z_{i,ox}}{Z_{i,fuel} - Z_{i,ox}} \quad (2.21)$$

and where,

$\overline{f'}$ = mixture fraction variance

σ_t, C_g, C_d = constants

Z_i = elemental mass fraction

S_m = source term, liquid to gas

The mixture fraction, along with the assumption of chemical equilibrium, allows chemistry to be reduced to a few mixture fractions related to species mass fractions, density, and temperature scalars. The mixture fraction variance is used in the closure model for turbulence-chemistry interactions [18].

Premixed combustion models make the assumption that combustion occurs in a flame sheet [20]. This flame sheet is defined by regions of burnt and unburnt species where the reaction progress variable determines the flame position. The propagating flame front is stretched by turbulence and determined from turbulent eddies and laminar flame speed. The flame front movement is defined by the transport equation of the progress variable,

$$\frac{\partial(\rho c)}{\partial t} + u_j \frac{\partial(\rho u_j c)}{\partial x_j} = \frac{\partial}{\partial x_i} \frac{\partial}{\partial x_i} \left(\frac{\mu_t}{S_{ct}} c \right) + \rho S_c \quad (2.22)$$

where,

S_{ct} = turbulent Schmidt number (0.7)

c = progress variable

ρS_c = mean reaction rate

The progress variable is defined as,

$$c = \frac{\sum_{i=1}^n Y_i}{\sum_{i=1}^n Y_{i,eq}} \quad (2.23)$$

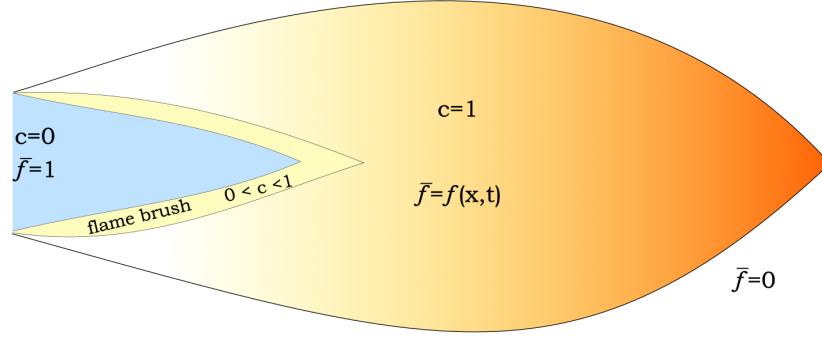


Figure 2.2: A diagram of Partially Premix variables within a flame

where,

$$n = \text{number of products} \quad (2.24)$$

$$Y_i = \text{mass fraction of product species} \quad (2.25)$$

$$Y_{i,eq} = \text{equilibrium mass fraction of product species} \quad (2.26)$$

The reaction mean rate (S_c) is defined as,

$$S_c = \frac{\rho_u}{\rho} U_t \left| \frac{\partial c}{\partial x_i} \right| \quad (2.27)$$

where,

$$\rho_u = \text{unburned density}$$

$$U_t = \text{turbulent flame speed}$$

The mixture is burnt ($c=1$) behind the flame front and unburnt ahead ($c=0$). Ahead of the flame front, the equilibrium mixture fraction (f) is calculated *a priori* using a probability density function of the range of mixture values. Unburnt gas properties, such as density and temperature, are curve fit to the mixture fraction PDF. Burnt gas properties are functions of the equilibrium mixture fraction and enthalpy due to the non-adiabatic nature of the flow. The mean reaction rate (S_c) in Eqs. 2.22 is based on turbulent flame speed (S_t) which is itself a function of laminar flame speed. As noted by Keating [40], the flame speed is an important parameter in defining premixed flame front position.

Turns [39] states that the conserved mixture fraction scalar, though useful in diffusion flames (i.e. non-premixed flames), provides no new information for premixed combustion because the mixture fraction is uniform everywhere and all species diffuse at the same rate. This is why the Partially Premixed model must use both the progress variable to determine where the flame front is inside the flame brush, and the mixture fraction variable to determine the species properties at a point in the domain.

2.5 Radiation

Discrete Ordinates radiation models solve the Radiative Transfer Equation (Eq. 2.28) for a number of discrete solid angles having a direction \bar{s} [18]. The RTE is transformed into a transport equation,

$$\frac{\partial I(\bar{r}, \bar{s})}{\partial x_i} + (a + \sigma_s)I(\bar{r}, \bar{s}) = an^2 \frac{\sigma T^4}{\pi} + \frac{\sigma}{4\pi} \int_0^{4\pi} I(\bar{r}, \bar{s}') \phi(\bar{s} \cdot \bar{s}') d\Omega' \quad (2.28)$$

$$\frac{\partial I_1 \bar{s}_1}{\partial x_i} + (a + \sigma_s)I_1 = an^2 \frac{\sigma T^4}{\pi} + \frac{\sigma}{4\pi} \sum_0^n I_j \phi_j \Delta\omega \quad (2.29)$$

Here,

λ = wavelength

a = spectral absorption

I = intensity

σ_s = scattering coefficient

ω = scattering coefficient

The transformed equation in Eq. 2.29 has the terms, from left to right, rate of change of radiation intensity, the absorption of radiation by the gas, the emission of radiation by the gas, and the scattering of radiation.

Looking at Figure 2.3, the left-hand side is an example of how gas irradiates the sample at an infinite number of angles for every point on the sample face. Discrete

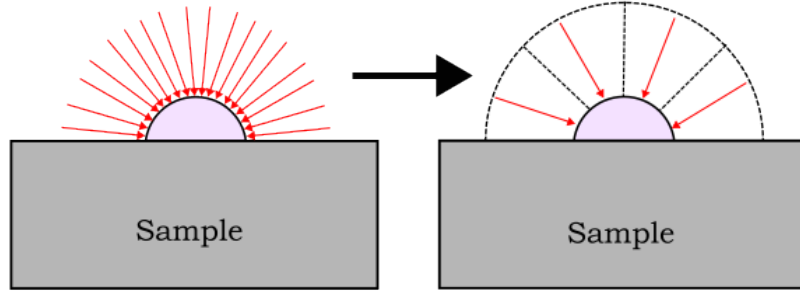


Figure 2.3: Infinite radiating beams converted to Discrete Ordinates sectors

Ordinates transform the RTE and reduce the scattering integral by only summing the intensities over a number of discrete sectors, as shown on the right-hand side of the figure. The uncoupled DO model sequentially solves energy and radiation intensities for every direction \vec{s} in the transformed transport equation. When radiation is coupled to the energy equation, objects, such as a sample, are assumed to be opaque therefore not transferring radiation back to the gas.

2.6 Discretization

Given the complex nature of the governing differential equations and the real-world geometries used, it is necessary to mathematically divide large areas into small regions thereby creating a mesh. Several ways exist to discretize a numerical domain. This study uses the Finite Volume method which simplifies the differential equations to their integral form, then to their algebraic equations. At every meshed volume cell-center the governing algebraic equations are solved for in a matrix of equations.

Chapter 3 Methodology

3.1 Overview

Two different methods for combustion and species transport were used in this study: the Eddy-Dissipation model and the Partially Premixed method. The flow variables are solved for, and validated against, experimental data from Miller-Oana [3], and Marra et al. [1]. ANSYS Design Modeler™, Meshing™, and Fluent™ were used to design the geometry, create the mesh, and solve the CFD equations, respectively.

To verify the assumptions for equilibrium and EDM were valid a “back of the envelope calculation” of Damköhler, based on calculations in Turns [39], was done. If $Da \gg 1$ then “fast” combustion occurs and reaction time is short allowing for wrinkled reacting sheets. This wrinkling induces high mixing and the “mixed is burnt” assumption is valid, thus neglecting complex chemical kinetics. However, if $Da \ll 1$ the combustion may be deemed “slow” and the flow is well-stirred such that chemical kinetics must be accounted for. At $Da = 0$ the flow is considered frozen and only occurs when the flow is so fast that the reaction does not have “time” to happen.

$$S_L = S_{L,ref} \left(\frac{T}{T_{ref}} \right)^\gamma \left(\frac{P}{P_{ref}} \right)^\beta \quad (3.1)$$

$$S_L = 136 \text{ cm/s} \quad (3.2)$$

β = function of equivalence ratio

γ = function of equivalence ratio

$S_{L,ref}$ = laminar flame speed at reference temperature

T_{ref} = reference temperature (298K)

P_{ref} = reference pressure (101kPa)

It was assumed that the pressure and temperature are only minimally changed from the reference to unburnt values such that the laminar flame speed is equal to the

reference laminar flame speed of 136cm/s [39]. The fuel was assumed to behave as air at 1800K which has a thermal diffusivity (α) of $482 * 10^{-6} \text{m}^2/\text{s}$ [41], at the average of burnt and unburnt temperatures. The flame thickness was then calculated from Eq. 3.3,

$$\delta = 2\alpha/S_L \quad (3.3)$$

$$\delta = \frac{2(482 * 10^{-6} \text{m}^2/\text{s})}{1.36 \text{m/s}} \quad (3.4)$$

$$= 0.7 \text{mm} \quad (3.5)$$

Therefore, the characteristic chemical time (τ_{chem}) is reduced to,

$$\tau_{chem} = \frac{\delta_L}{S_L} \quad (3.6)$$

$$\tau_{chem} = 0.52 \text{ms} \quad (3.7)$$

The characteristic flow time (τ_{flow}) was found by rearranging the formula for turbulent intensity 2.12 for the root-mean-square velocity u' and applying a turbulent intensity of 4.5%, and an average velocity of 100ms. It is also assumed that the integral scale (l_0), which characterizes the largest eddy size, is approximately half the length of the potential core, or 1cm, because the eddies occur downstream of the nozzle. Substituting these in to the characteristic flow equation,

$$\tau_{flow} = \frac{l_o}{u'} = \frac{1 \text{cm}}{0.045(u_{avg})} \quad (3.8)$$

$$\tau_{flow} = \frac{10 \text{mm}}{0.045(100 \text{m/s})} = 2.2 \text{ms} \quad (3.9)$$

Where,

α = thermal diffusivity

β = function of equivalence ratio

γ = function of equivalence ratio

$S_{L,ref}$ = laminar flame speed at reference temperature

c_p = specific heat

l_o = integral turbulence scale

P_{ref} = reference pressure (101kPa)

Finally, we resolve the Damöhler number in Eq. 2.15,

$$Da = \frac{\tau_{flow}}{\tau_{chem}} = \frac{2.2\text{ms}}{0.52\text{ms}}$$

$$Da \approx 4.3$$

As shown, the Damöhler number is indeed larger than one and it may be assumed that combustion proceeds whenever excessive turbulence is present [17][18]. This simplification confirms assumptions made by equilibrium and the EDM methods.

The overall methodology for this study is shown in the flow chart in Figure 3.1. First, cold flow (i.e. no combustion) was run until convergence criteria were met. This establishes appropriate flow variables in the domain and is used as input for combustion. Next, the volumetric species with Eddy Dissipation and Relax to Chemical Equilibrium solver was turned on and ignited by patching the domain with a small amount of products - 0.1 CO₂ and 0.1 for H₂O.

3.2 Experiment discussion

Several experiments for combustion and ablation were investigated for this research. The two main experiments that will be discussed and validated are the Miller-Oana et al. [3] and the Marra et al. [1].

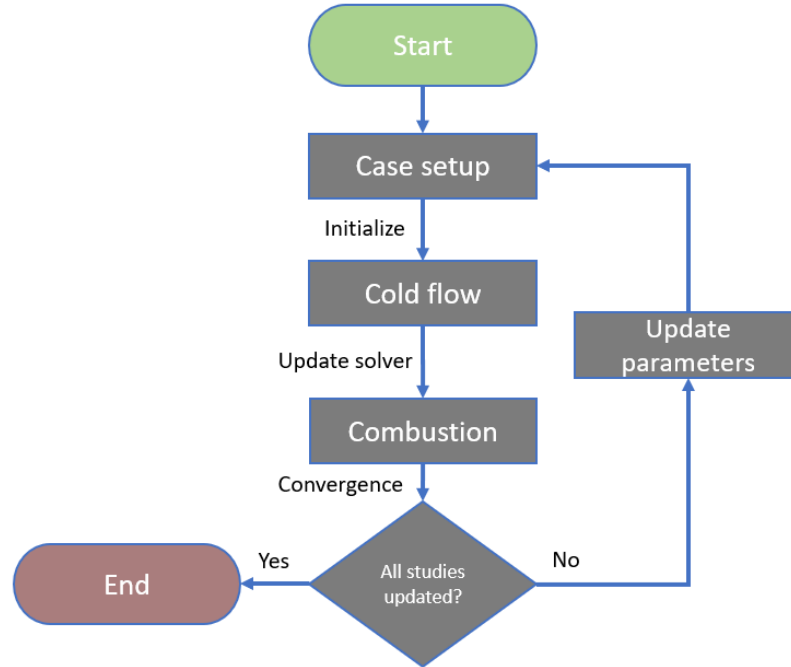
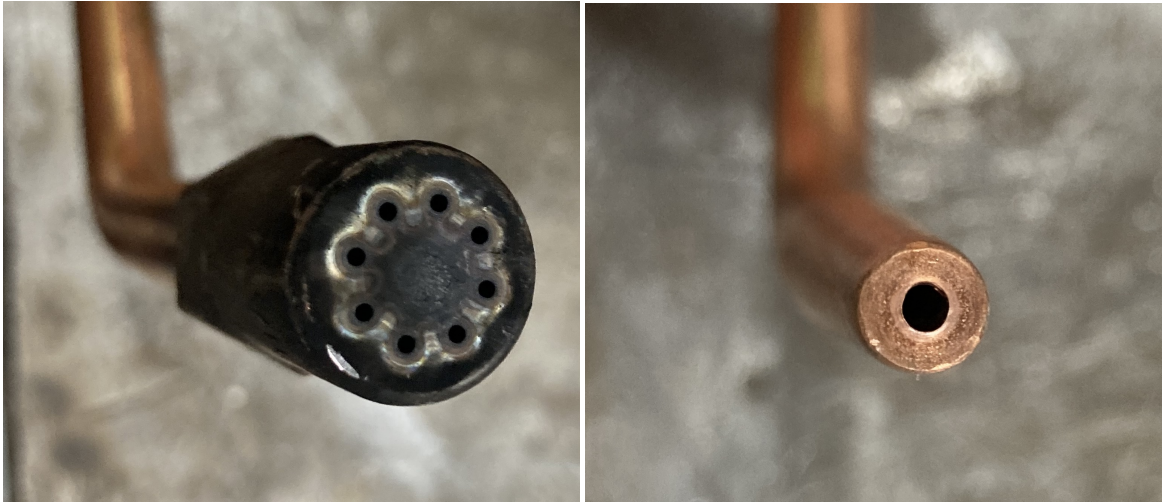


Figure 3.1: Parametric study flowchart

Unlike some experiments, such as the one by Aydin et al. [22] whose torch used a heating tip (Figure 3.2a), Miller-Oana and Marra used a welding tip (Figure 3.2b) which uses a singular hydraulic diameter. Both tips have a torch body with a mixing chamber that blends the oxygen and acetylene prior to exit allowing the flow field upstream of the torch tip to not have to be modeled. This reduction simplifies the geometry and resolves the concern of pre-ignition inside a tip domain due to turbulent mixing; an issue due to assumptions in the EDM combustion model. The Eddy-Dissipation model ignites whenever turbulence becomes high, therefore a nozzle domain would cause a nonphysical flashback to occur.

Gardon gauges were used in both experiments to measure heat flux. These devices have a black sensor in the middle of a copper plate and are kept cool using a liquid with thermocouples attached to the center sensor and the cool wall. The temperature difference changes the resistance of the thermocouples allowing for the heat flux on the sample to be calculated from the voltage change.



(a) Heating tip example

(b) Welding tip example

Figure 3.2: Torch tip comparison



Figure 3.3: Torch body example

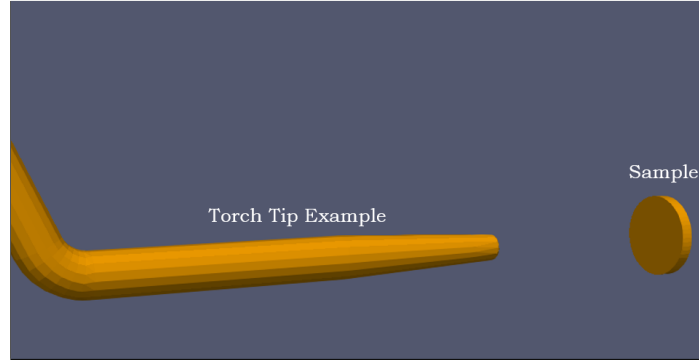


Figure 3.4: 3-D Geometry

3.3 Geometry creation

The created geometry was based on the documented apparatuses from Miller-Oana and Marra. The mesh was changed from the 3-D Geometry (Fig.3.4) to a 2D axisymmetric geometry to reduce computation requirements; as shown in Fig.3.5. The fluid domain was drawn as a rectangle surrounding the sample material domain and is sectioned by projection lines to aid in the meshing process. A small line measuring the diameter of the tip was set as the fuel inlet, and distances from the torch tip and the diameter of the torch tip were varied depending on the experiment.

Marra did not provide detailed descriptions of the welding torch used in their experiment; however, based on readings of the work and images provided it is assumed that a Mecor N #6.5 ($\varnothing 2.814\text{mm}$) [42] welding tip was used. This type of welding tip had the closest drill size to the reported hydraulic diameter, and a shape matching the images in the paper. The distance from the tip to the sample was set at 4.5mm as specified in the paper. The Miller-Oana experiment used a Victor welding tip #4 ($\varnothing 1.854\text{mm}$) and the distance of the sample from the torch tip was varied from 5mm, 7mm, 9mm, and 11mm.

3.4 Mesh and grid independence

A structured H-grid type was used to increase the speed of calculations given the complexity and small scale of combustion problems. The structured grid allows for

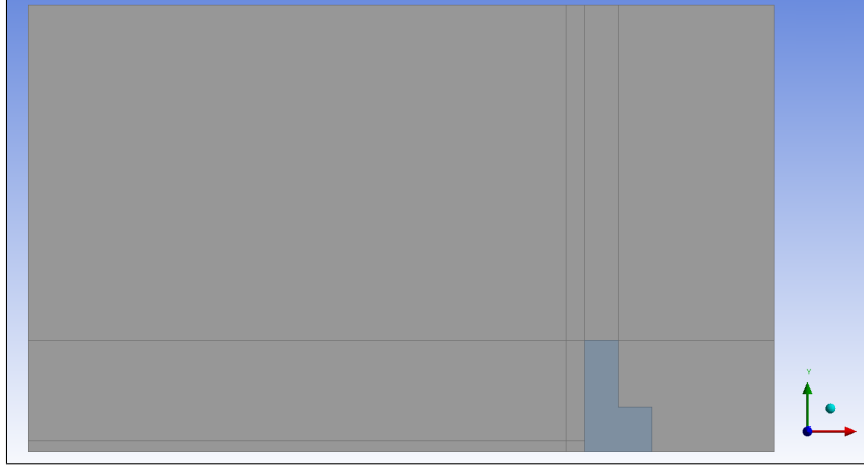


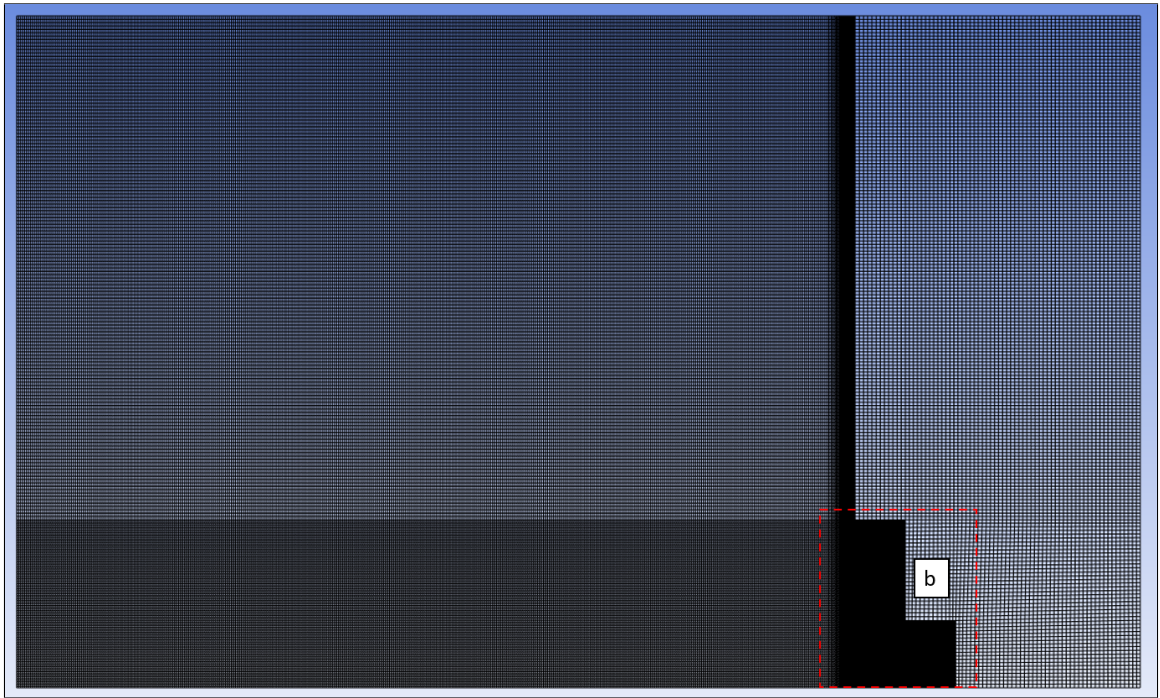
Figure 3.5: Geometry

Table 3.1: Mesh cell count

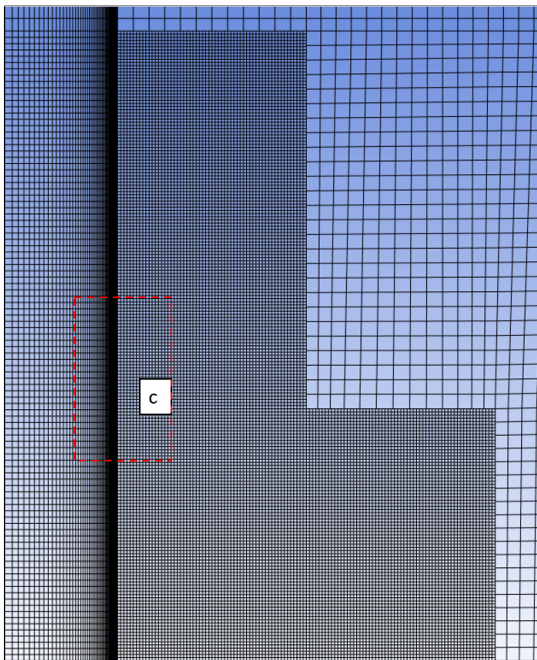
Domain	Cell count for Miller-Oana validation	Cell count for Marra validation
Fluid	125363	100363
Solid	16800	16800
Total	142163	117163

quicker calculation through better memory management due to better orthogonality, skewness, and Jacobian transforms.

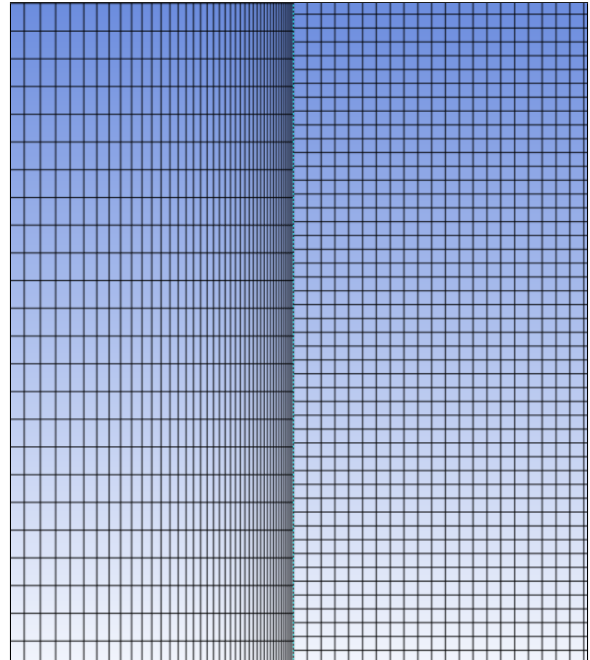
Between the solid sample and the fluid domain, a non-conformal mesh was used that allowed the fluid mesh to be refined to capture the complex nature of the boundary layer, while the solid mesh is kept more course. The non-conformal mesh adds complexity to the model due to the misalignment of the fluid domain and the solid domain, as shown in Figure 3.6c; however, the solver automatically adds interfaces between these domains which act as a coupled wall. This misalignment is easily seen in Figure 3.6c. A decrease in computations was seen by removing the sample domain and fixing temperature values for a single face; however, no large difference in heat flux occurred during trials. The non-conformal grid was kept to allow for dynamic meshing in the future. A coarse mesh was used for the sample as the internal domain was less important and held at a constant temperature. A secondary mesh was created to the dimensions of the SigrathermTM sample and is shown in Figure 3.8 to validate against the Marra ablative sample.



(a) Model Mesh



(b) Sample Mesh



(c) Boundary layer mesh

Figure 3.6: An overview of the entire fluid and solid domain mesh, (a) Overview of mesh, (b) sample mesh, (c) boundary layer

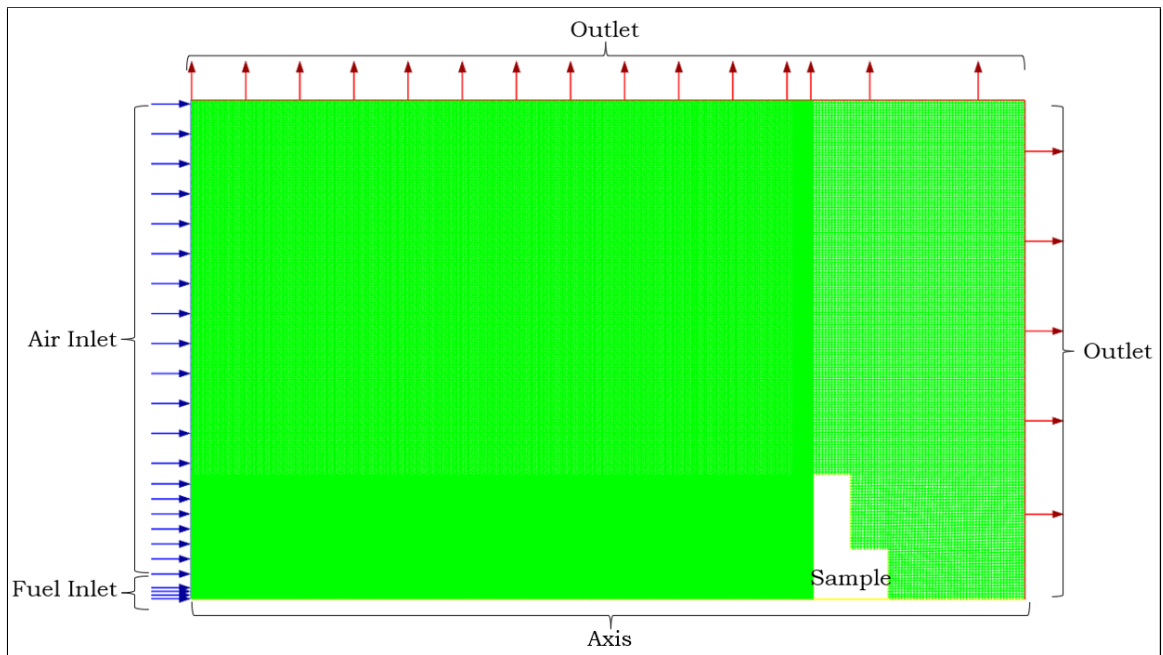


Figure 3.7: Boundary location and descriptions for the domain with a gauge.

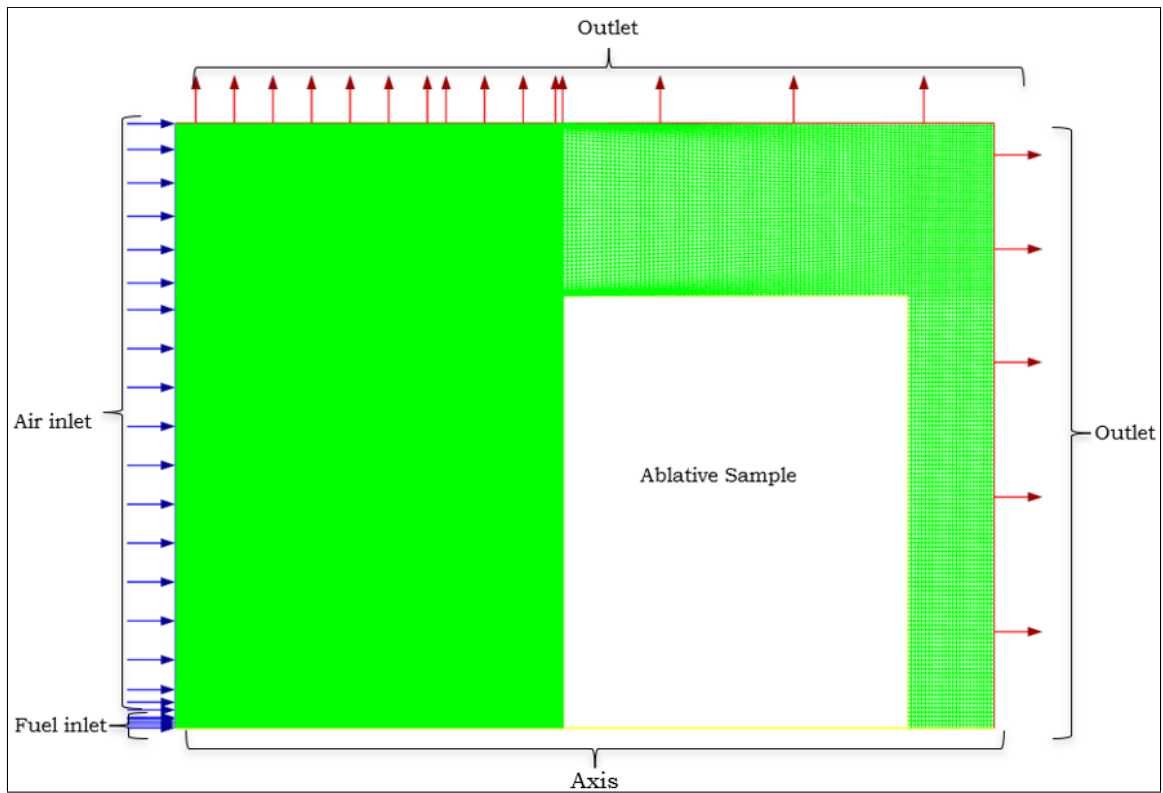


Figure 3.8: Boundary location and descriptions

To ensure that the flow conditions on the sample were captured appropriately, a grid study was completed where wall y^+ was monitored and kept below unity to predict accurate heat transfer results. The boundary layer mesh was modified along with the distances near-wall in the parametric grid study. Then, a cold flow model was run where wall y^+ and cell count were compared. It was found that the bias of the inflation layer, not the number of divisions along the flow nor the inflation layer division quantity, was extremely important. To balance the computation demands and accuracy, the mesh used 400 divisions along the flow with an inflation layer of 50 divisions and a bias factor of 15.

3.5 Solver

The solver used in this work was pressure-based and assumed steady state with the coupled pressure-velocity coupling scheme. Gravity was included and set in the negative y -direction to account for buoyancy. To solve for heat transfer into the sample the energy equation was set, as well as the discrete ordinates solver for radiation. Intermediate combustion and intermediate solid heat transfer processes were irrelevant to this study, allowing for the assumption of a steady state with pseudo-time stepping. The $k - \omega$ SST model was selected to close turbulence and allowed for both accurate prediction of turbulence in the far field and in the viscous layer near-wall.

The chemistry model was modified to relax reactions to chemical equilibrium for EDM, and to accelerate the intensive chemistry equilibrium calculations the In Situ Adaptive Tabulation [43], or ISAT, algorithm was used. The table created by the algorithm is stored as a binary tree where the leaves consist of an initial composition, a reaction mapping, a mapping gradient, and a hyper-ellipsoid of accuracy; the nodes consist of cutting planes. Linear interpolation is used to find the current value of the new entry from the previous entry value. It is faster to calculate new values from the interpolated values and quickly retrieve them from a binary tree than it is to calculate the values during the solver steps. During the initial setup, the binary tree size was

increased to 500Mb to allow more values to be stored and finer interpolation.

The Partially Premix model was also investigated in this study and used chemical equilibrium calculations to simplify the chemistry. The default model was changed to non-adiabatic so that radiation is accounted for, and the Fuel Stream Rich Flammability limit was set to 1 to cover all ranges of fuel mixture in the probability calculations. The boundary conditions were manually modified to account for the variable VFR of the fuel stream while the oxidizing stream was kept at atmospheric mass fractions. Before the probability density function table was created, the initial number of grid points was increased to 20 to allow for more granularity. This probability density function (PDF) calculates the chemistry properties for each mass fraction as described in the governing equations.

EDM using direct source calculations for chemical reactions was briefly investigated as well. This method resulted in longer computation times, larger flame temperatures, higher heat flux, greater velocities, much lower partial pressures of oxygen, and a nonphysical flow potential core. These are documented issues with using EDM that seemed to be exacerbated by the flow velocities. Therefore, EDM using direct source chemistry calculation was not used in the study.

3.5.1 Initial conditions

Solid domain

The sample domain was assumed to be made entirely of isotropic copper with ANSYS Fluent™ default properties. The solid domain was then fixed with a temperature value at 393.15 and 300K for Marra, and Miller-Oana, respectively.

During the ablative test cases, the solid material was changed to Sigratherm® to align with the experiment and CFD done by Marra et al. The material properties for the ablative sample were listed by Marra et al. and taken by performing laser flash measurements[1]. These properties are input as a new material (D) without a fixed temperature.

Fluid domain

The fluid was set to be either acetylene-air or a pdf-mixture for the Eddy-Dissipation model and Partially Premixed models, respectively. The acetylene-air mixture was modified from the default mixture to have a density set as an “ideal gas”; all other properties remain as the defaults. A custom gas mixture was created during the setup of the Partially Premix model. This mixture contained species and properties that were calculated by the solver. The air temperature was set to be 300K, while the oxy-fuel temperature was set to 298K.

3.5.2 Boundary conditions

The boundary conditions were similar for both turbulent chemistry models used but the setup was modified according to the experiment requirements.

Air inlet

It was assumed that all experiments investigated in this work take place in a controlled environment with little air movement because ambient air conditions were not recorded in either experiment. To allow atmospheric air to constantly enter the domain with a molar fraction of 21% oxygen and 79% nitrogen (minor atmospheric species were ignored), an inlet velocity of 0.1m/s with a turbulence intensity of 1% was set to model the quiescent atmosphere.

Fuel inlet

Oxyacetylene fuel exits the tip with a flow rate and species mass fraction depending on the VFR modeled. The appropriate mass flow and mass fractions were calculated using a given VFR by obtaining the volumetric flow rate, in standard liters per minute, for oxygen and acetylene from the investigators and inserting into Eqs. 3.10 and 3.11. A reference temperature (T_{ref}) of 294K and a pressure ratio of unity for both streams

Table 3.2: Miller-Oana Fuel Inlet Conditions

VFR	Mass Flow Rate (kg/s)	O2 Mass Fraction	C2H2 Mass Fraction
1.35	7.10E-04	0.62	0.38
1.5	7.60E-04	0.65	0.35
1.75	7.60E-04	0.68	0.32

Table 3.3: Marra Fuel Initial Conditions

Mass Flow Rate (kg/s)	O2 Mass Fraction	C2H2 Mass Fraction
2.15E-04	0.44	0.56

were assumed.

$$\dot{V}_{lpm,gas} = \dot{V}_{slpm,gas} \rho_{gas} \frac{T_{gas}}{T_{ref}} \frac{P_{gas}}{P_{ref}} \frac{0.001m}{60s} \quad (3.10)$$

$$\dot{m}_{gas} = \rho_{gas} \dot{V}_{lpm,gas} \quad (3.11)$$

To calculate the mass flow for each constituent in the fuel, the density for acetylene and oxygen was calculated from the ideal gas law to be 1.077 kg/m³ and 1.325 kg/m³ for oxygen. Using Eq. 3.11 a mass flow for each species was calculated and summed as the total mass flow. This is summarized in Table 3.2. The mixture density, and dynamic viscosity (μ), were assumed to be 1.07kg/m³ and 1E-5 Pa-s. The Reynolds number calculated from Eq. 2.14 is approximately 40,000, making the turbulent intensity, therefore, approximately 4.5% from Eq. 2.12.

Marra fuel boundary conditions were calculated by taking the mass flow conditions for each stream and dividing by the sum, as in Eq. 3.12 and are summarized in 3.3.

$$w_{o2} = \frac{\dot{m}_{o2}}{\dot{m}_{c2h22} + \dot{m}_{o2}} \quad (3.12)$$

$$w_{c2h2} = \frac{\dot{m}_{c2h22}}{\dot{m}_{c2h2} + \dot{m}_{o2}} \quad (3.13)$$

Pressure outlet

A Pressure Outlet boundary condition was used to the top and right side of the domain. To account for the reintroduction of fluid into the domain, a “backflow”

Table 3.4: Boundary condition summary

	Fuel Inlet	Air Inlet	Outlet
Velocity (m/s)	-	0.1	-
Mass Flow (kg/s)	variable	-	-
Turbulent Intensity	4.5%	1%	5%
Hydraulic Diameter	0.18542 cm	-	-

condition was set as the atmospheric at an ambient temperature of 300K. The turbulent intensity was left as the default of 5% due to the lack of concern about back-flow into the domain.

Axis

All domains in the study were a mirror image along the x-axis and therefore set as an axis boundary condition. By using the axis boundary we reduce the numerical domain substantially without affecting the computations or results. The flow and thermal conditions are mirrored along the axis such that zero flux occurs along the boundary; a safe assumption because the flow is averaged.

3.5.3 Initialization and calculation

Relaxation and pseudo-time stepping parameters were set to control divergence in the flow. Pseudo-time stepping was utilized as a relaxation factor where there is a different time step size in every cell. The fluid time step was set to 0.01 seconds, and the solid time step was set to 0.1 seconds. The larger time step was set for the solid because heat transfer is slower in the material than in the flow. The flow was initialized with hybrid initialization, and the atmospheric oxygen mass fraction was patched into the domain. The solver was run and the residuals and sample wall face pressure were monitored until convergence was achieved. The flow was determined to be converged when the wall pressure reached a steady state and the residuals for all variables reached 1E-6 or until they repeated.

Chapter 4 Results and discussion

Marra [1] and Miller-Oana [3] are experimental studies used to validate the model result and both experiments followed the ASTM E285-80 [8] standard with slight variations. The flow conditions of oxygen and acetylene streams were monitored before being thoroughly mixed in the torch body mixing chamber and exiting the nozzle.

To validate against the Marra et al. experiment one EDM case was run against the copper gauge geometry, and two cases, one with EDM and one with Partially Premixed, were run against the ablative sample geometry. The experiment did not modify any input parameters so those remained constant in all the cases.

To validate against the Miller-Oana et al. experiment, twelve cases were executed using the EDM Relax to Equilibrium model using a parametric study within ANSYS Workbench™ and twelve Partially Premixed models were executed manually. Input parameters were set that modified the distance from the nozzle tip to the sample, the fuel inlet mass flow rate, and the species mass fractions according to the VFR being studied. When the geometry was modified accordingly, it would then be re-meshed and updated in the solver along with the updated solver parameters. Automatic Initialized and Case Modification settings were set up such that each case could be run with no user involvement. This would allow the solver to run continuously and remove possible user interaction errors. Residuals and variables of interest could be monitored during the run as needed.

4.1 Marra experiment

This study found similar results using EDM with relaxation to chemical equilibrium compared with the Marra et al. Eddy Dissipation Concept approach. The overall potential core and flame front align well with the experiment and are due to the

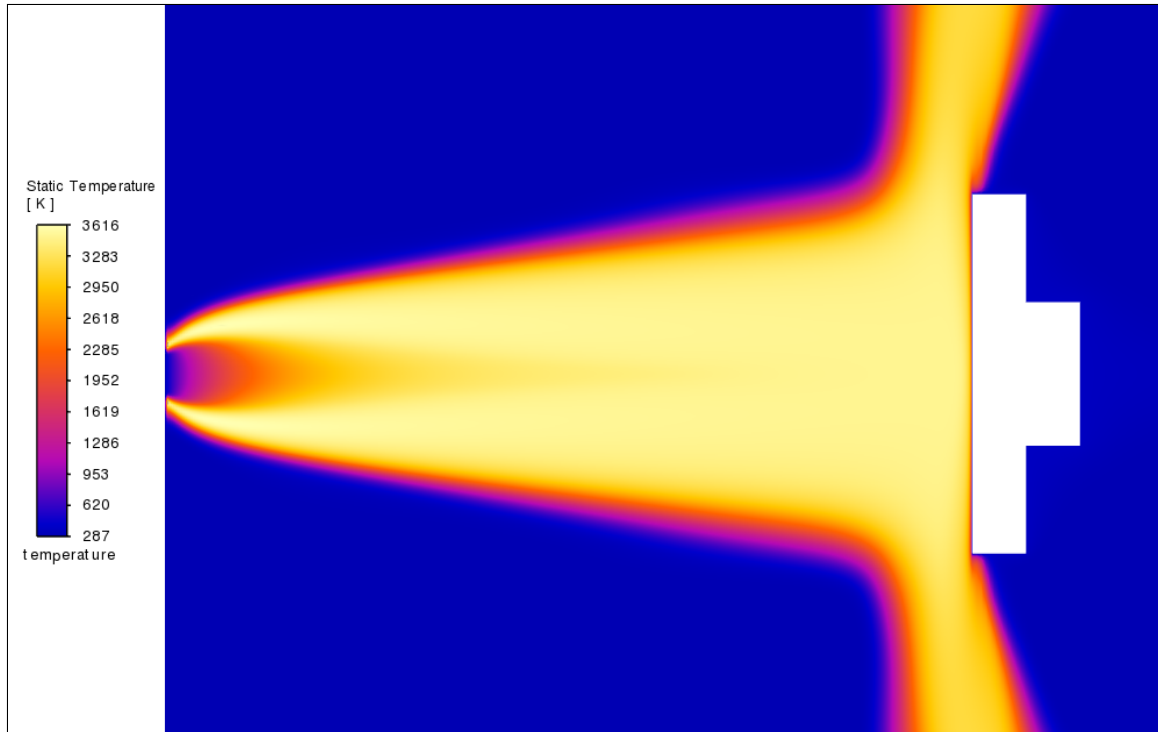


Figure 4.1: Eddy-Dissipation Method temperature contour plot spanning 4.5cm from nozzle tip to sample wall

reduction in exit velocity. There was good alignment between maximum temperatures shown in the temperature profile (Figure 4.1), and adiabatic temperatures reported for oxyacetylene combustion. The maximum flame temperature is in good agreement with the 3580K reported by Marra et al. using the EDC method. It should be noted here that the flame is a carburizing flame and the maximum temperatures calculated by EDM are still higher than adiabatic temperatures at that equivalence ratio. The Partially Premixed flame temperatures align more with expectations.

Heat flux values using EDM are in very good agreement with those reported by Marra et al.[1] and in good agreement with Fortner et al.[2]. The experimental data showed a range of 150-160 W/cm² and a CFD measurement of 158 W/cm². This work found the heat flux on the sample was on the higher end of the reported values at 159.82 W/cm², due to model simplifications and species reduction. The turbulent reaction rate is shown in Figure 2.27 and shows the areas of reaction for the EDM flame. As expected, the highest reaction rate occurred in the area of the premixed

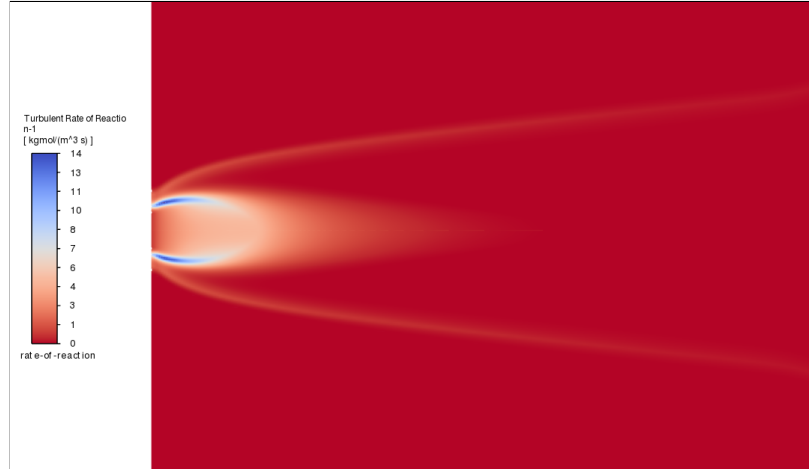


Figure 4.2: Turbulent rate of reaction contour plot

flame. However, the outer part of the flame has a slight increase due to the turbulent mixing of atmospheric oxygen with the high-temperature products.

The pressure profiles for both combustion models of this study are shown in Figure 4.3. Although there is no validation for these profiles they were checked to make sure the result is physical. Pressure is shown to rise to a maximum of 200Pa above atmospheric, which is plausible at the velocities of the flow.

Wall y^+ is shown in Figure 4.4 and showed that the viscous sub-layer should be adequately resolved for the copper gauge case as the values are below unity.

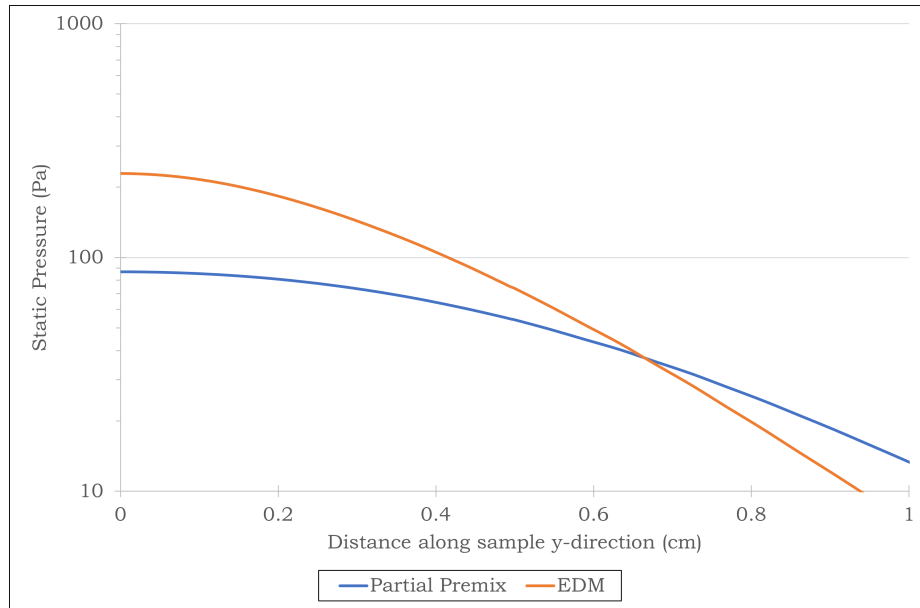


Figure 4.3: Pressure profile along the copper gauge face

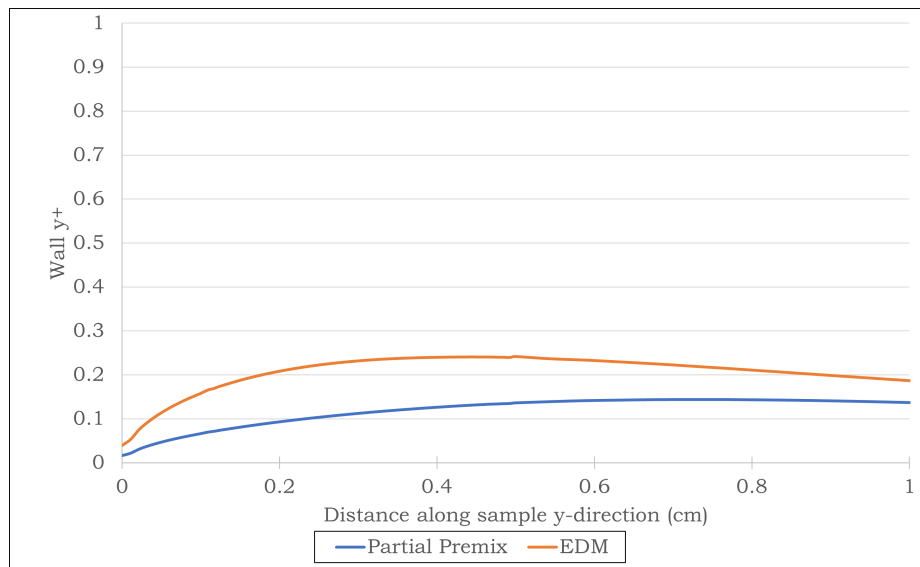


Figure 4.4: Wall y+ along the face of the copper gauge case

Table 4.1: Gauge and ablative sample result comparison with Marra et al.[1] and Fortner [2]

	Marra Experiment	Marra CFD	Fortner	This Study-EDM	This Study-Partially Premixed
Copper Gauge					
Heat flux (W/cm ²)	150-160	158	153	159.8	-
Flame temperature (K)	-	3580	3245	3616	2928
Ablative Sample					
Heat flux (W/cm ²)	-	-	-	168.9	71.5
Face temperature (K)	1970-2070	1900	1800	1769	1560
Back temperature (K)	630	850	-	958	927

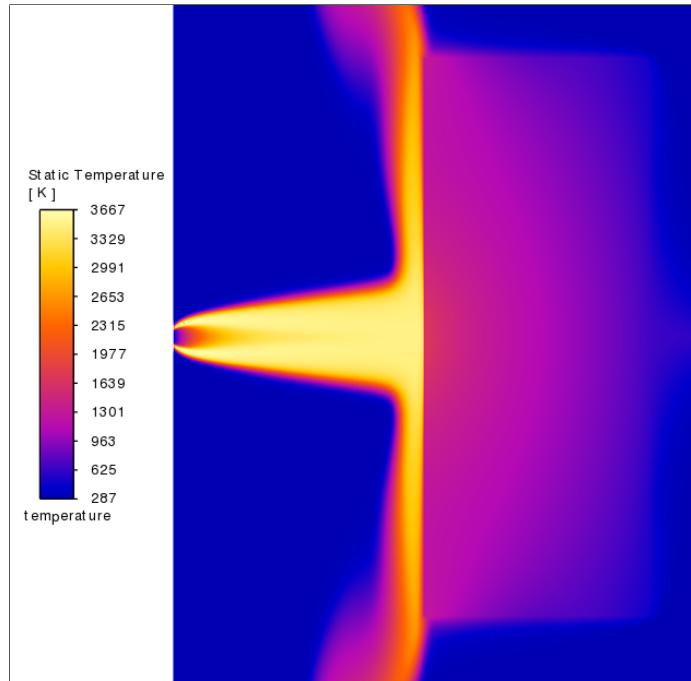
Table 4.2: Computational requirement comparison of Marra et al. [1] and this study for the gauge study

	Copper Gauge		Ablative Sample
	Marra	This study-EDM	This study-Partially Premixed
Iterations	900000	6500	11000
Run time (min)	12513	79.8	62.7

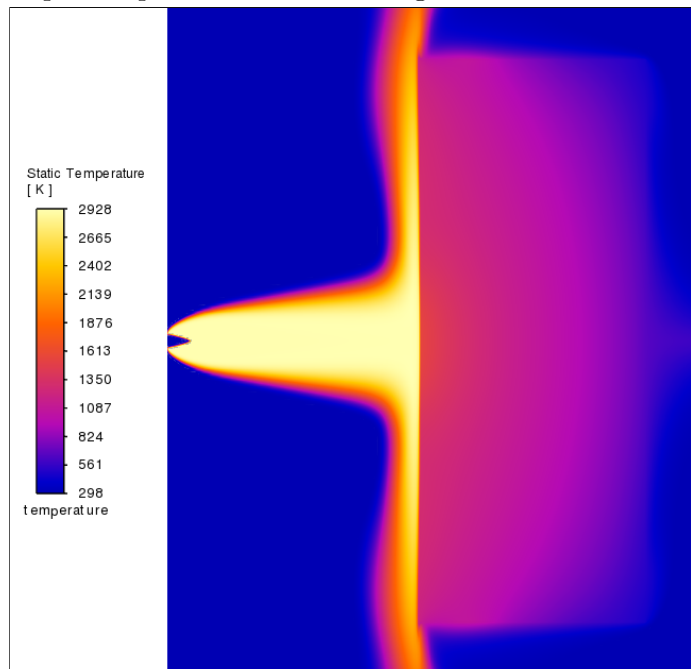
Once the heat flux and other flow properties were measured from the copper gauge, the ablative CFD simulation was run. The temperature contours of the fluid and sample are shown in Figure 4.5. As expected, the EDM temperature is higher than adiabatic and the Partially Premixed temperature is much lower in comparison. As mentioned earlier, the flame is a reducing, or carburizing, flame therefore a lower flame temperature is expected. The internal temperatures of the Sigratherm™ sample are shown in Figure 4.6 and have contours with the greatest temperature at the stagnation point and dissipating outward toward the back face.

Shown in Figure 4.7 is the internal temperature of the ablative sample along different paths away from the axis of the sample. The EDM with relaxation to equilibrium method is compared to the results from the EDC method used by Marra. The front face temperatures are very well aligned with the CFD results from Marra except the back face (i.e. 10cm from the actual back face to the experimental thermocouple) temperatures tend to be higher by 100K to 75K. Actual back temperatures predicted from this study align well with the back face temperature from the experiment; though, Marra reported that the thermocouple never reached a steady state. The Partially Premixed paths were not captured due to the fact no experimental data was listed from the report only CFD data. Because both EDC and EDM over predict flame temperature they would not have produced a good source of verification for the Partially Premixed model.

An Intel(R) Core i7 processor and 16GB of RAM (same as Marra) was used to solve the flow with significant reductions in iterations performed and computation time; see Table 4.2. The assumptions made in the study allowed a large reduction in

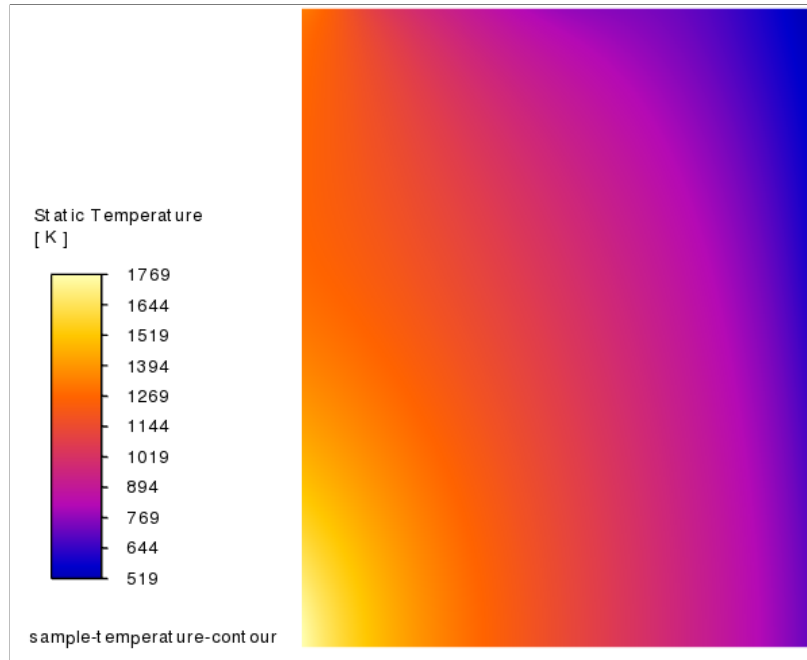


(a) Fluid and sample temperature contour using EDM with relaxation to equilibrium

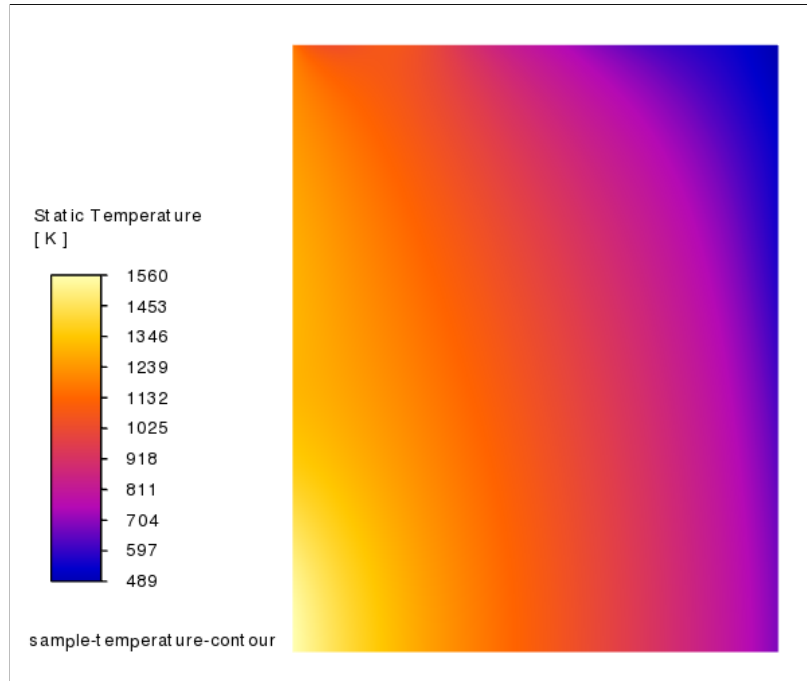


(b) Fluid and sample temperature contour using a Partially Premix model

Figure 4.5: Temperature contours of both fluid and solid domains using EDM Relation to Equilibrium (a) and Partially Premix combustion models (b)



(a) Interior of sample temperature contour using EDM with relaxation to equilibrium



(b) Interior of sample temperature contour using Partially Premix model

Figure 4.6: Interior temperature contours of an Sigratherm[®] sample using EDM Relation to Equilibrium (a) and Partially Premix combustion models (b)

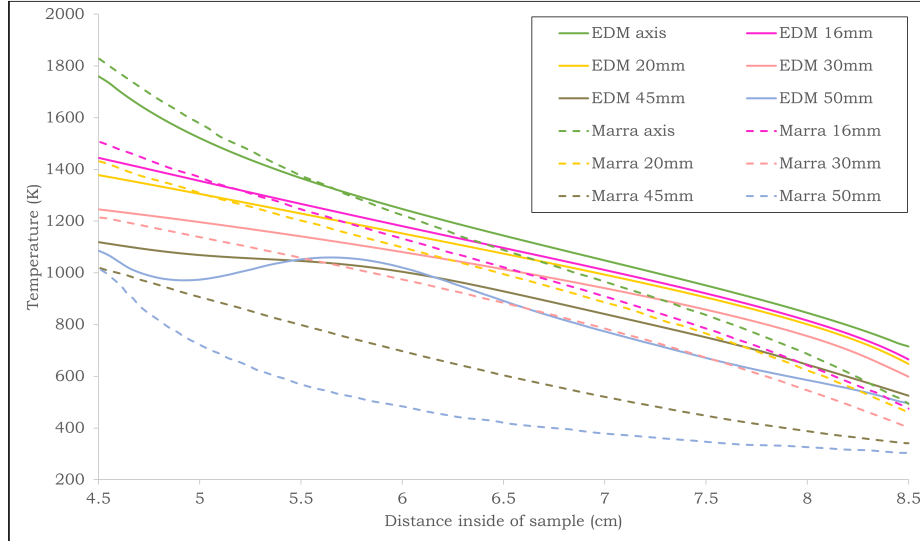


Figure 4.7: Ablative sample internal temperatures at various distances from the axis using EDM compared to Marra’s CFD results

iterations, from 900,000 iterations in the Marra CFD [1] work to 6,500 in the current work. The final results of this work are compared to Marra’s experiment, CFD, and Fortner’s CFD [2] and summarized in 4.1 for both all cases.

4.2 Miller-Oana experiment

At each distance, the heat flux, velocity, and partial pressure of oxygen were measured and a copper heat flux gauge was constantly cooled to 300K. To validate the results for partial pressure oxygen in the solver, a custom function was created. Pressure defaulted to Pascals in the solver and a conversion to kilopascals was added.

Flame temperatures using Eddy-Dissipation methods are often higher than adiabatic flame temperatures [36] [37] and can be seen in Figure 4.10a. The Partially Premixed model has a more realistic flame temperature compared to EDM due to the calculation of the mixture fraction based on pressure and temperature. Miller-Oana reported adiabatic flame temperatures from JANAF as 3300K for a stoichiometric mixture.

Initial models of this study used the Eddy-Dissipation model with direct-source chemistry source terms; meaning, chemistry source terms are used explicitly [33] in-

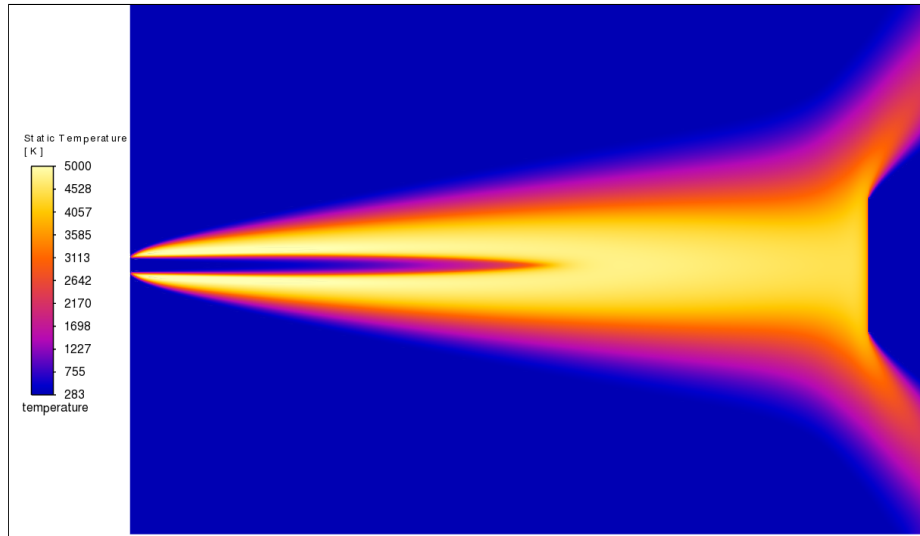
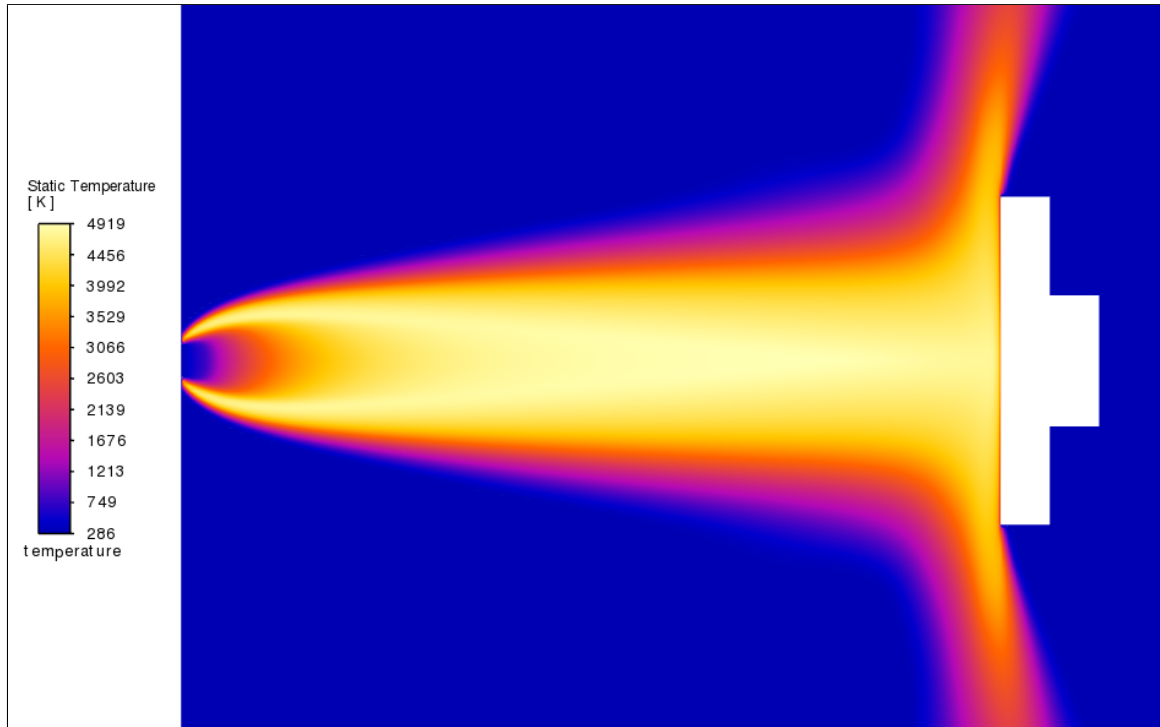


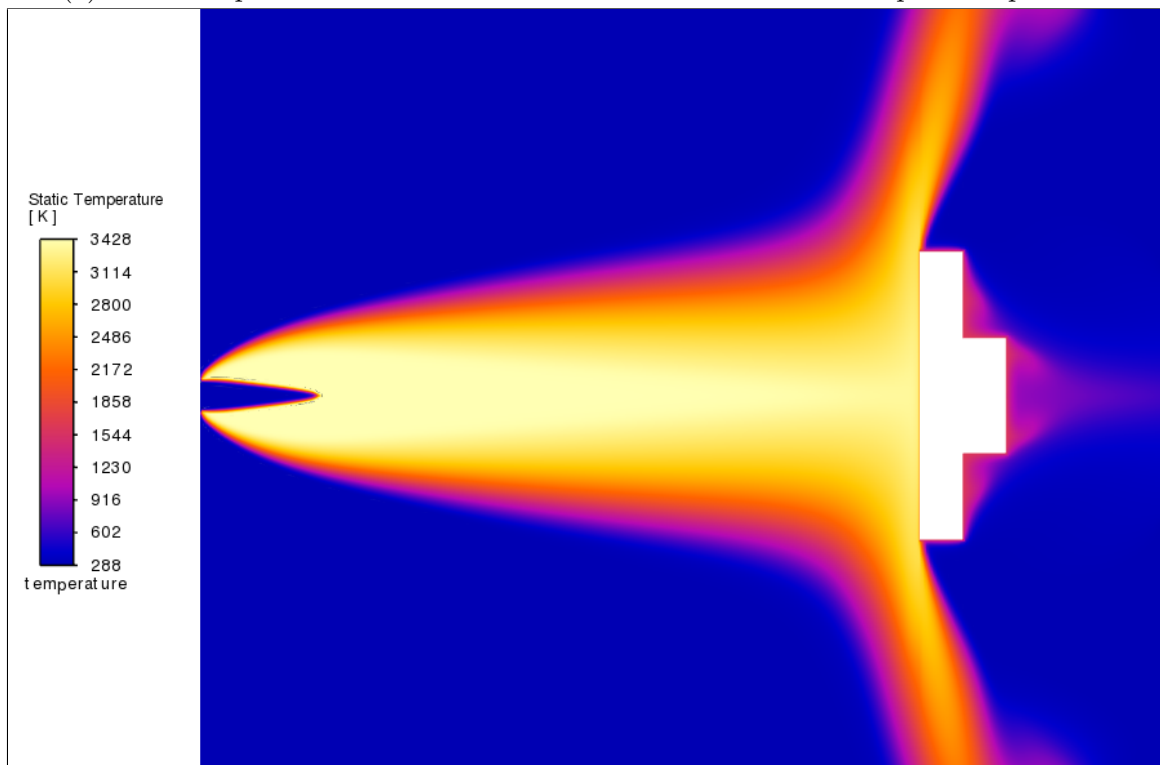
Figure 4.8: Temperature contour plot of the Eddy-Dissipation Model using direct-source terms in the species transport equation

stead of being reduced to equilibrium mass fractions. Therefore, the reaction variable of the species transport equation 2.6 is the lesser of the equations below when solving chemistry. The potential core of the flow and the flame length extended further downstream than is physical and is shown in the temperature contour of Figure 4.8. This phenomenon causes incorrect partial pressure and velocities in the flow. After many cases and further reading, it was determined that this method yields non-physical results for the flame profile. The contours and output for the intermediate sample distances, 7cm and 9cm, and the VFR's 1.5 and 1.7, are shown below for a visualization of how the flow changes for different distances and flow conditions. For all the images it is shown that as the VFR increases (as oxidizer is increased) the flame temperature withdraws toward the torch tip along with a decrease in temperature. This recession was also noted by Miller-Oana et al.[3].

Heat flux is one of the most important variables when investigating ablation. Proper heat flux estimates affect the material recession and flow parameters near the sample. The values in Figure 4.22 follow the decreasing trend from experiment data, and align better the further from the nozzle tip. At the furthest distances Figure 4.23 shows the maximum heat flux does not occur at the stagnation point for greater

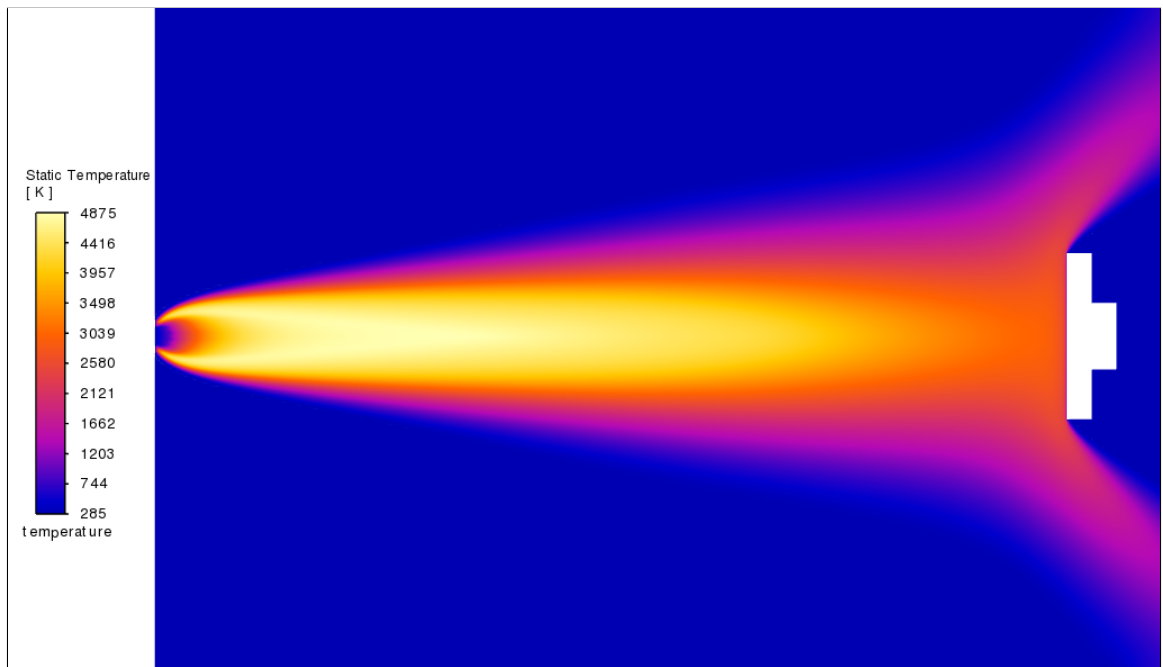


(a) EDM temperature contour of 1.35 VFR at 5cm from nozzle tip to sample wall

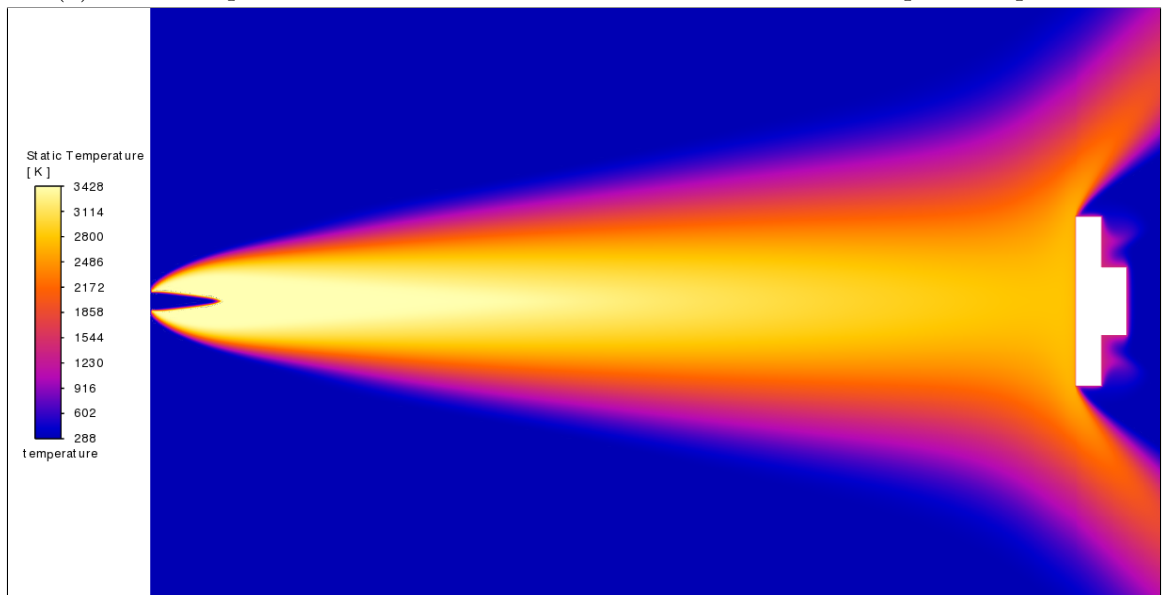


(b) Partially Premix Model temperature contour plot of 1.35 VFR at 5cm from nozzle tip to sample wall

Figure 4.9: Temperature contours at a distance of 5cm from nozzle tip to sample wall with 1.35 VFR for EDM (a) and Partially Premix combustion models(b)



(a) EDM temperature contour of 1.35 VFR at 11cm from nozzle tip to sample wall



(b) Partially Premix Model temperature contour plot of 1.35 VFR at 11cm from nozzle tip to sample wall

Figure 4.10: Temperature contours at a sample distance of 11cm and a VFR of 1.35 for EDM (a) and Partially Premix combustion models (b)

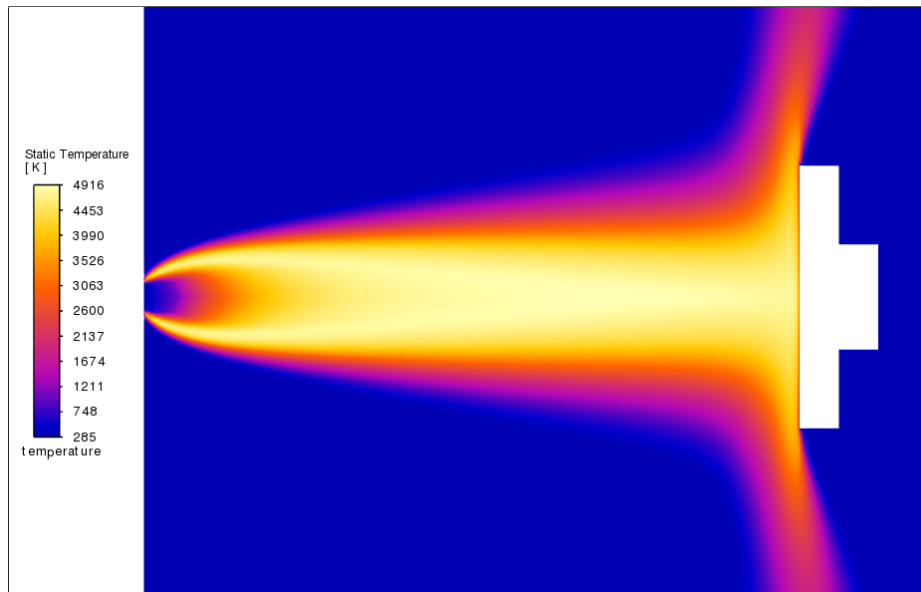


Figure 4.11: EDM temperature contour of 1.5 VFR at 5cm from nozzle tip to sample wall

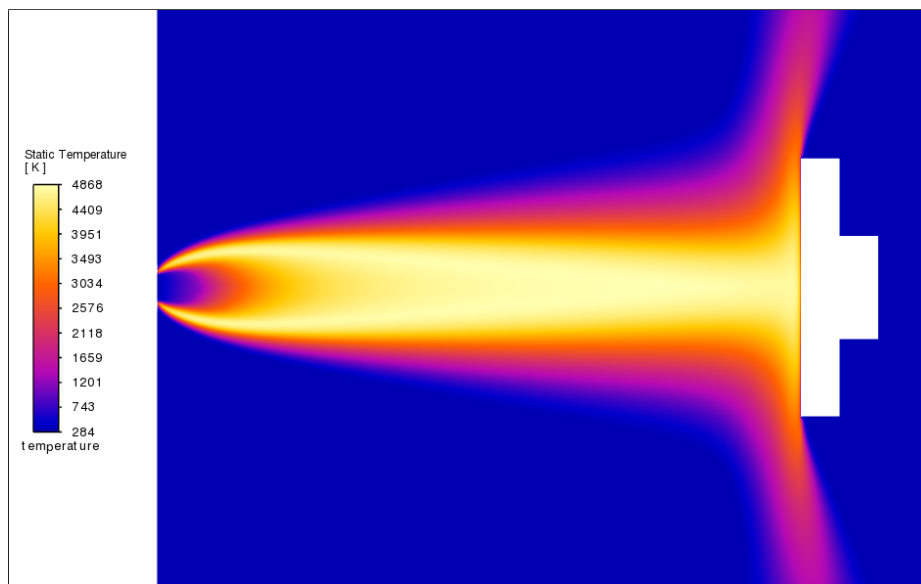


Figure 4.12: EDM temperature contour of 1.7 VFR at 5cm from nozzle tip to sample wall

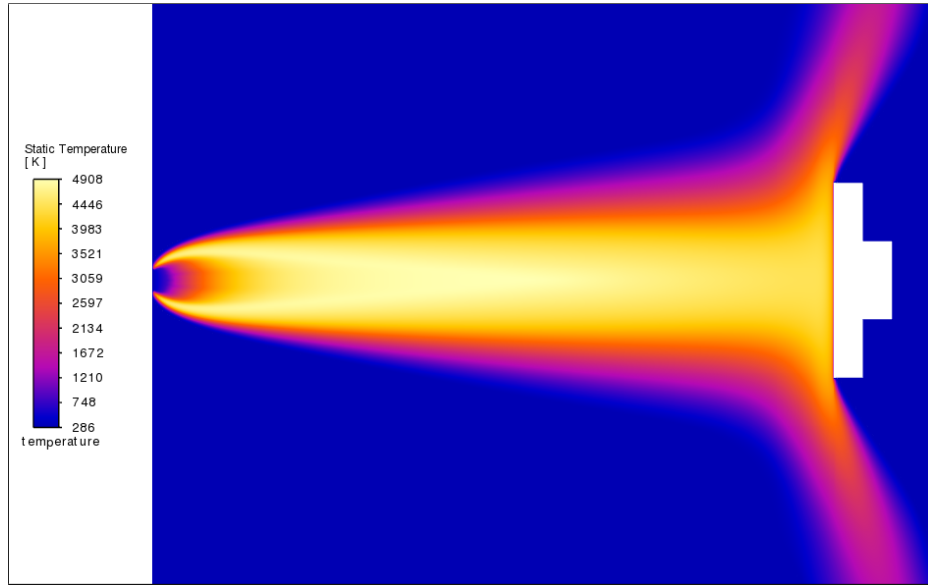


Figure 4.13: EDM temperature contour of 1.35 VFR at 7cm from nozzle tip to sample wall

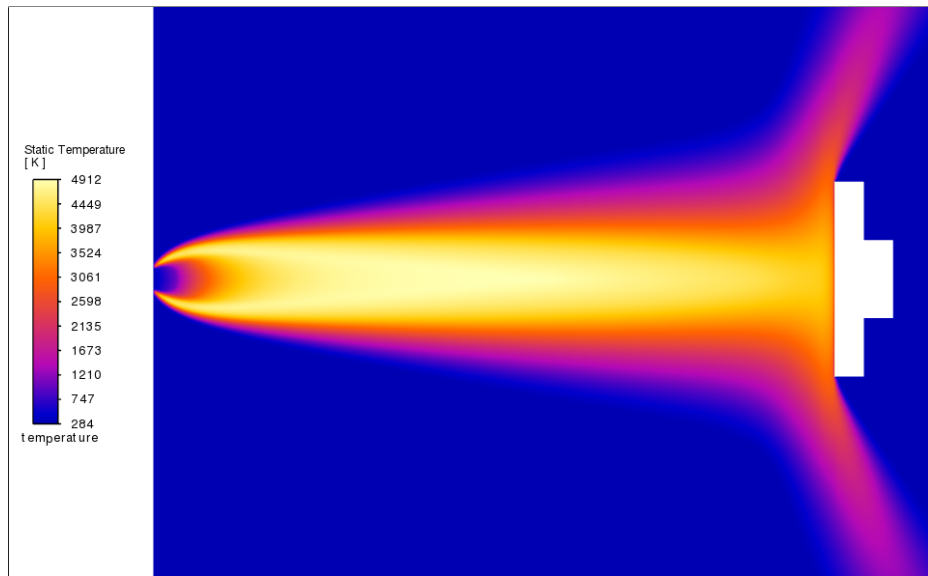


Figure 4.14: EDM temperature contour of 1.5 VFR at 7cm from nozzle tip to sample wall

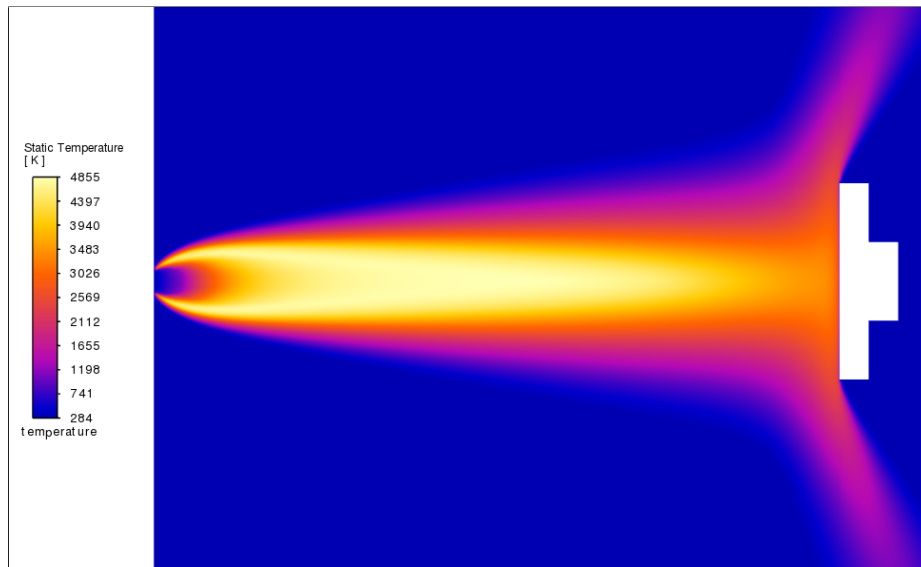


Figure 4.15: EDM temperature contour of 1.7 VFR at 7cm from nozzle tip to sample wall

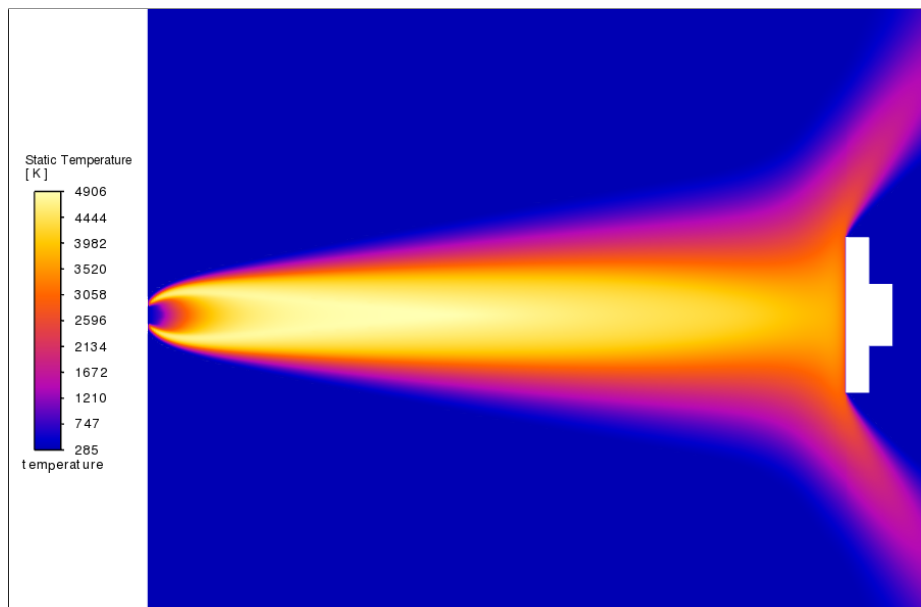


Figure 4.16: EDM temperature contour of 1.35 VFR at 9cm from nozzle tip to sample wall

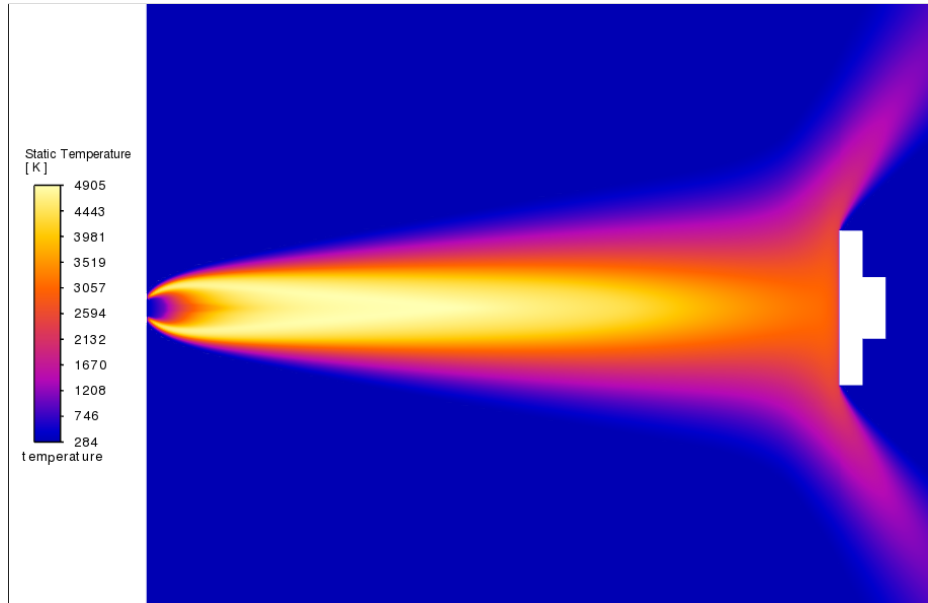


Figure 4.17: EDM temperature contour of 1.5 VFR at 9cm from nozzle tip to sample wall

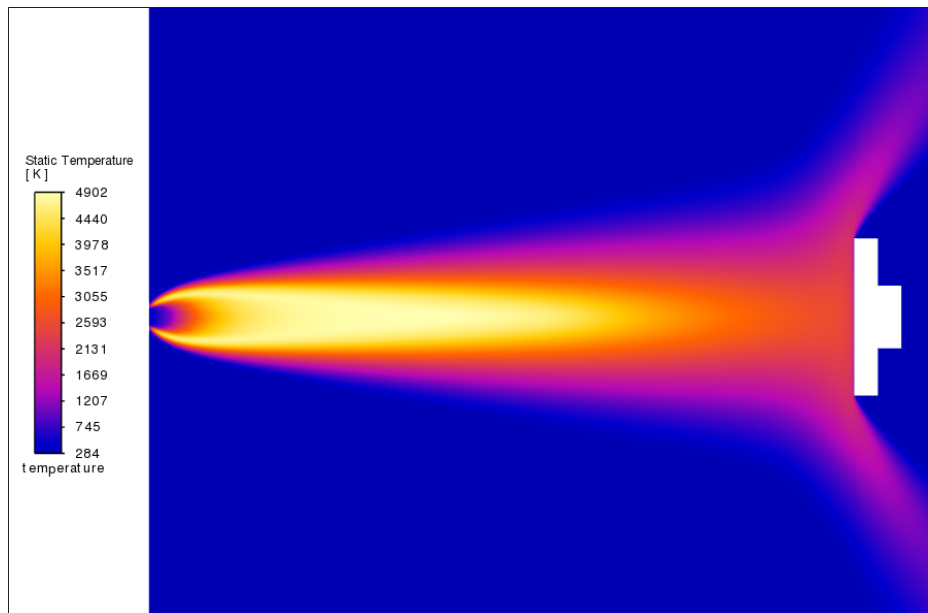


Figure 4.18: EDM temperature contour of 1.7 VFR at 9cm from nozzle tip to sample wall

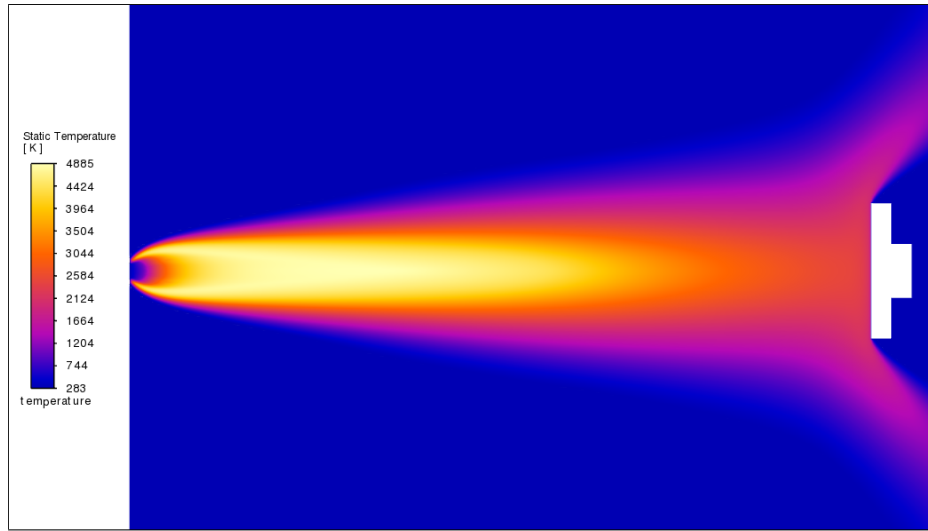


Figure 4.19: EDM temperature contour of 1.5 VFR at 11cm from nozzle tip to sample wall

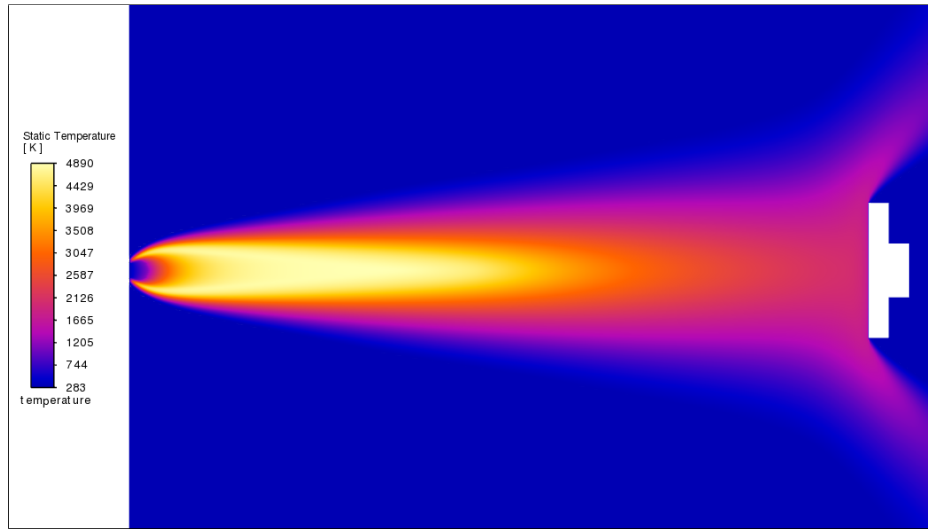


Figure 4.20: EDM temperature contour of 1.7 VFR at 11cm from nozzle tip to sample wall

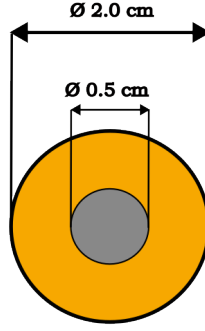


Figure 4.21: The front face of a Gardon heat flux gauge with a small sensor area surrounded by cooled copper.

distances from the nozzle. Spikes in heat flux at this location are physical but go away as the material is rounded upward through an ablation process. The ablation process is not modeled so the spike stays. It should be noted here that the Partially Premixed model does not allow the solid temperature to be fixed, as was the case with the EDM model, and heat flux was not able to be investigated or validated with experimental data.

The discretized area-weighted average of the heat flux was taken using the estimated sensor area of a Gardon gauge as shown in Figure 4.21. The heat flux over each cell of the sample face is multiplied by the facet area and divided by the total area of the sensor, as shown in Eq. 4.1. This average is displayed in the profile heat flux plot figures Figures 4.23.

$$\dot{q}_{avg} = \frac{\int q dA}{A} \approx \frac{\sum_{i=1}^n \dot{q}_i A_i}{A} \quad (4.1)$$

where,

A_i = annulus area

A = total sensor area

\dot{q}_i = cell heat flux

The velocities along the axis are compared to the data given by Miller-Oana et al. The Partial Premix model fits well with the data; whereas, the EDM model

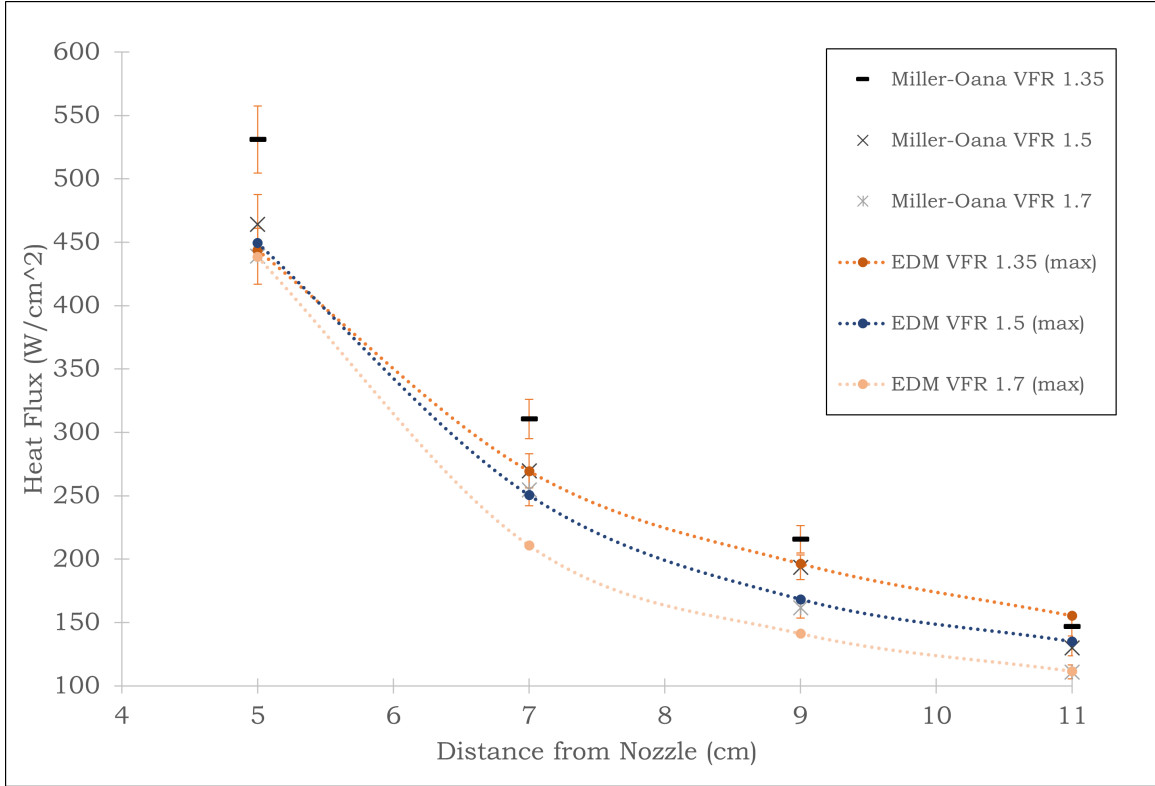
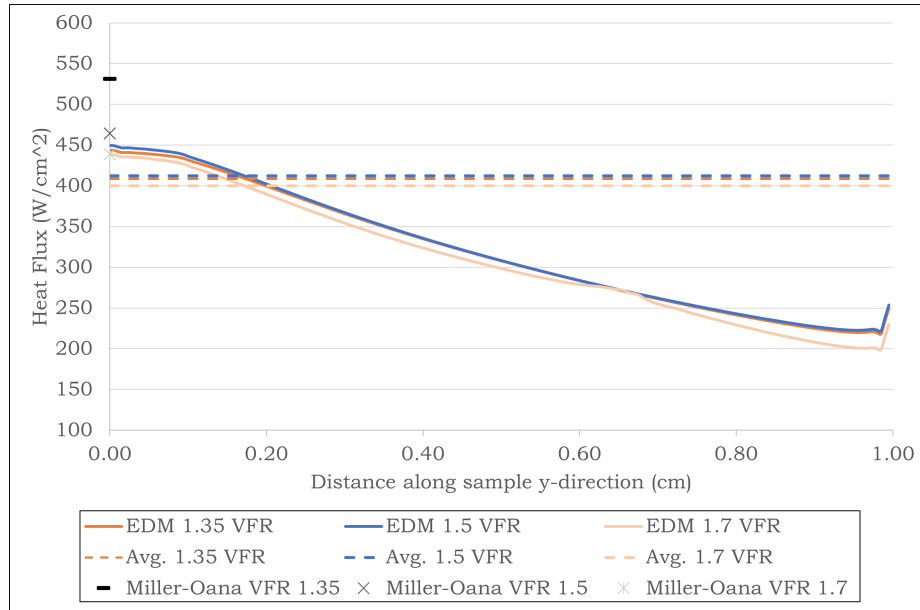


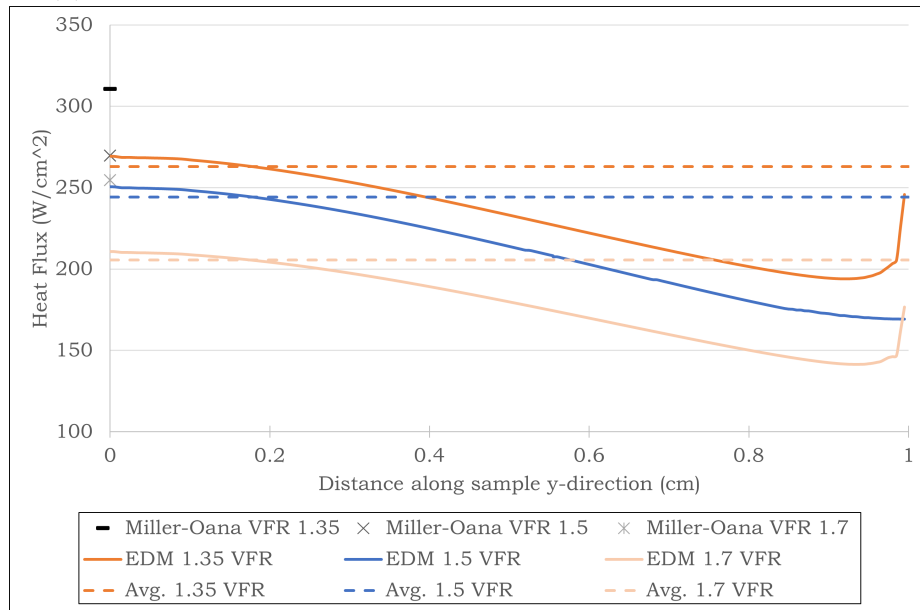
Figure 4.22: A comparison of heat flux values from 1.35, 1.5, and 1.7 VFRs at distances from 5cm to 11cm.

overpredicts the experiment data. According to Incropera et al. [41] the length of an impingement jet potential core should occur at $5D_h$, or 1cm for this study. By comparing both potential cores shown in the temperature contours (Figures 4.10b and 4.10a), both models show flame front has a great impact on the velocity along the axis.

The Partially premix model aligns reasonably well, especially at greater distances from the exit; cold flow velocity was provided as a reference. Both models have an initial spike of velocity followed by a sudden drop. This is due to the sudden increase in temperature and decreased density around the nozzle exit and flame front. From Figure 4.24 we can see that (A) corresponds to cold reactants entering the flame, and (B) is where we see an increase in velocity due to a change in density and temperature in the pre-heat region. Between (B) and (C) we see a sudden spike and drop in velocity due to the exothermic reaction and creation of products. This quasi-discontinuity

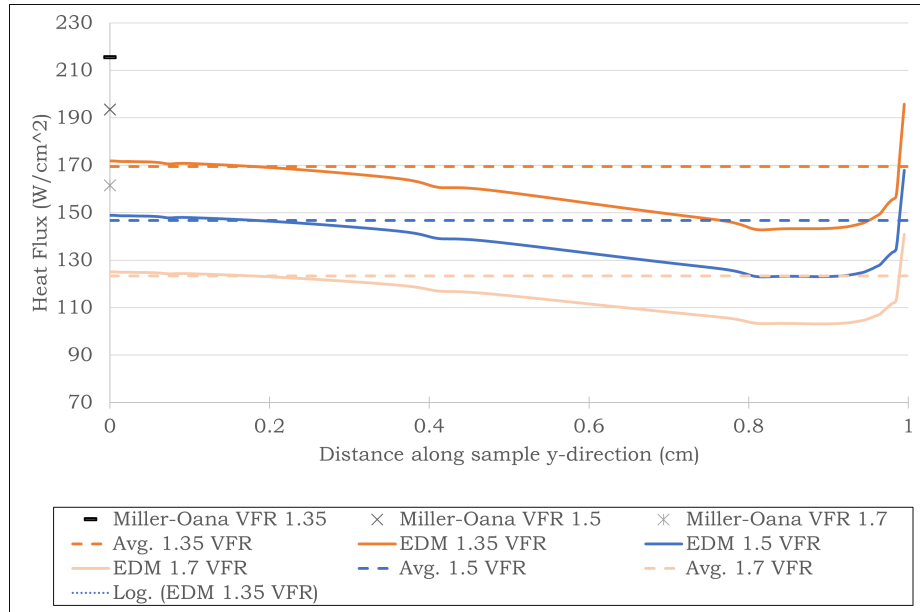


(a) Heat flux profiles on sample face at a 5cm from the nozzle tip.

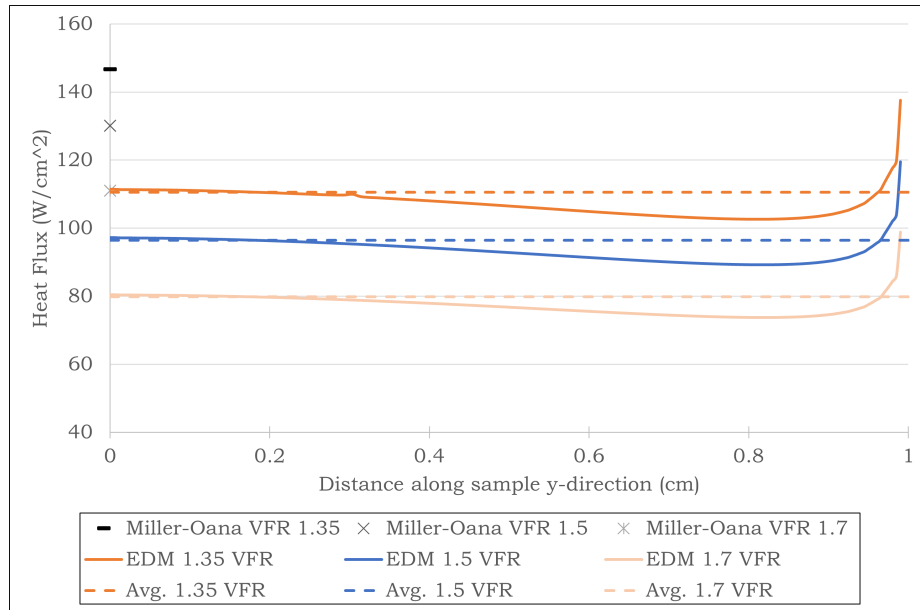


(b) Heat flux profiles on sample face at a 7cm from the nozzle tip.

Figure 4.23: Different VFR heat flux profiles on the face of the sample at distances of 5cm (a), 7cm (b), 9cm (c), and 11cm (d)



(c) Heat flux profiles on sample face at a 9cm from the nozzle tip.



(d) Heat flux profiles on sample face at 11cm from the nozzle tip.

Figure 4.23: Different VFR heat flux profiles on the face of the sample at distances of 5cm (a), 7cm (b), 9cm (c), and 11cm (d)

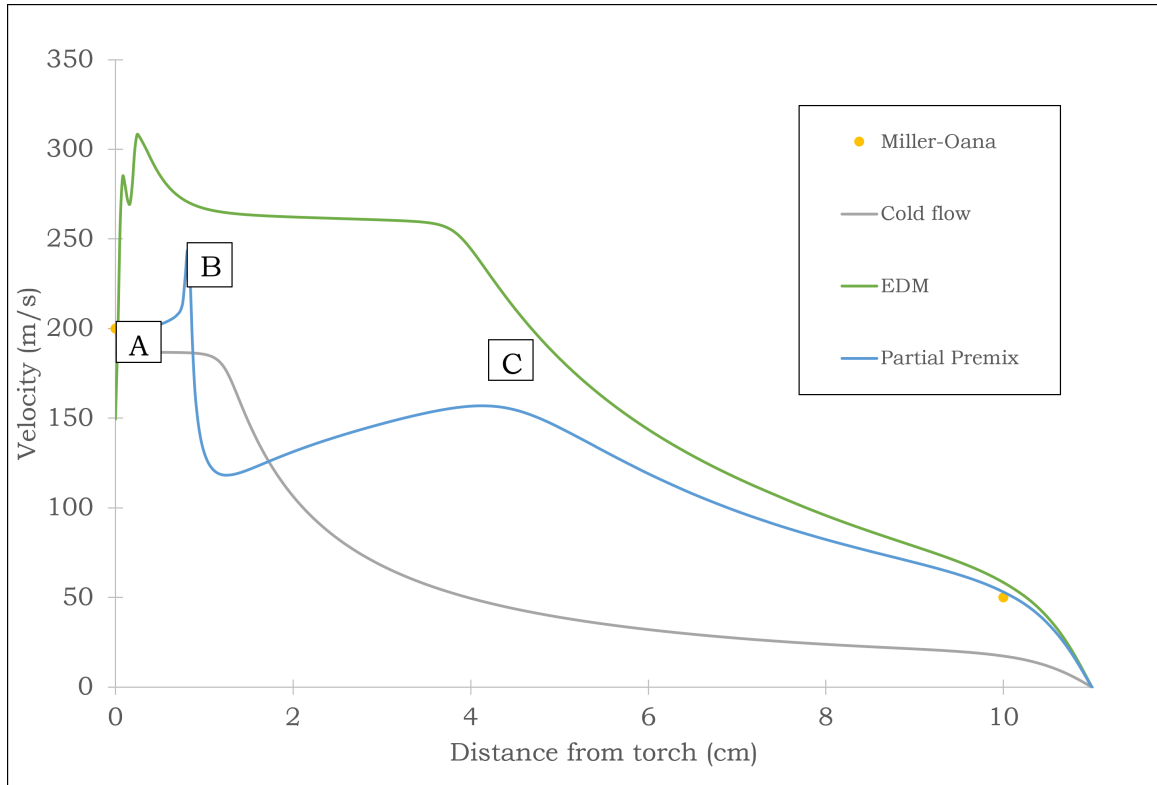
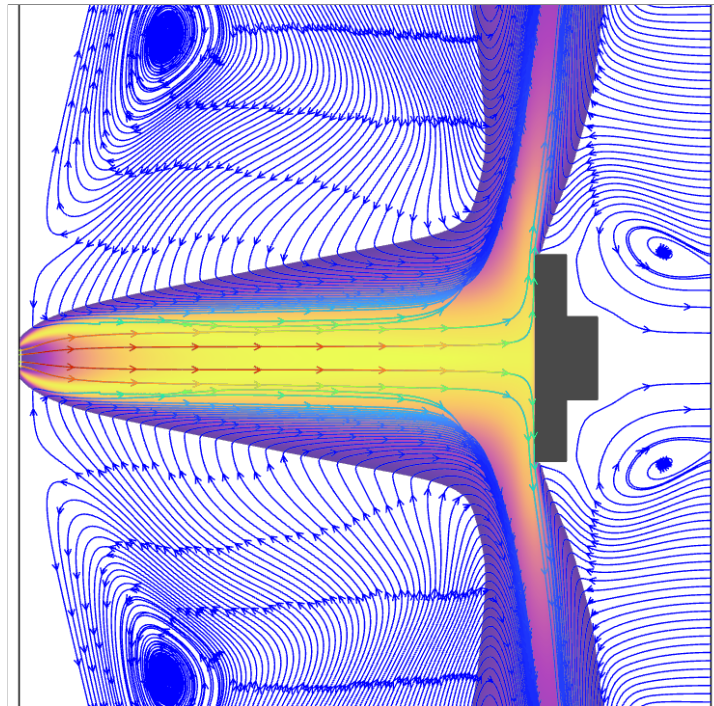


Figure 4.24: Velocity comparison graph of non-reacting flow, Eddy-Dissipation Model, Partially Premixed Model, and Miller-Oana et al. where (A) cold reactants (B) pre-heat zone (C) secondary ignition

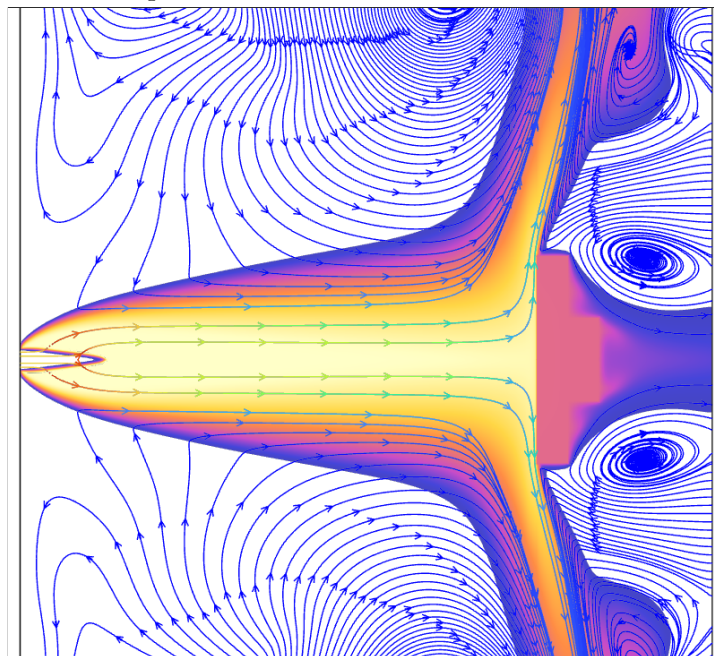
is the flame front which spans only a few millimeters before the products appear according to the mixture fraction computed. Velocity increases again at (C) due to the secondary combustion of entrained atmospheric oxygen and hot products. There occurs a gradual decrease in velocity where the products are cooled and momentum is lost.

The high temperatures in the flow cause moderate velocity gradients due to buoyancy. Looking at Figure 4.25b, the sample has heated due to the flame and has caused the relatively stagnant air in the back to move faster causing higher vorticity. This increase in vorticity is more prominent when comparing Figure 4.25b to Figure 4.25a where some vorticity exists due to the upward movement of the jet arm, however, not as much.

Partial pressures of oxygen are important to ablation to understand how oxida-



(a) Eddy-Dissipation model velocity pathlines overlaid on the temperature contours



(b) Partially Premixed model velocity pathlines overlaid on the temperature contours

Figure 4.25: Temperature contour overlaid by velocity pathlines at 5cm from the torch tip to sample with a 1.35VFR using Partially Premixed model (b), and the Eddy-Dissipation model(a)

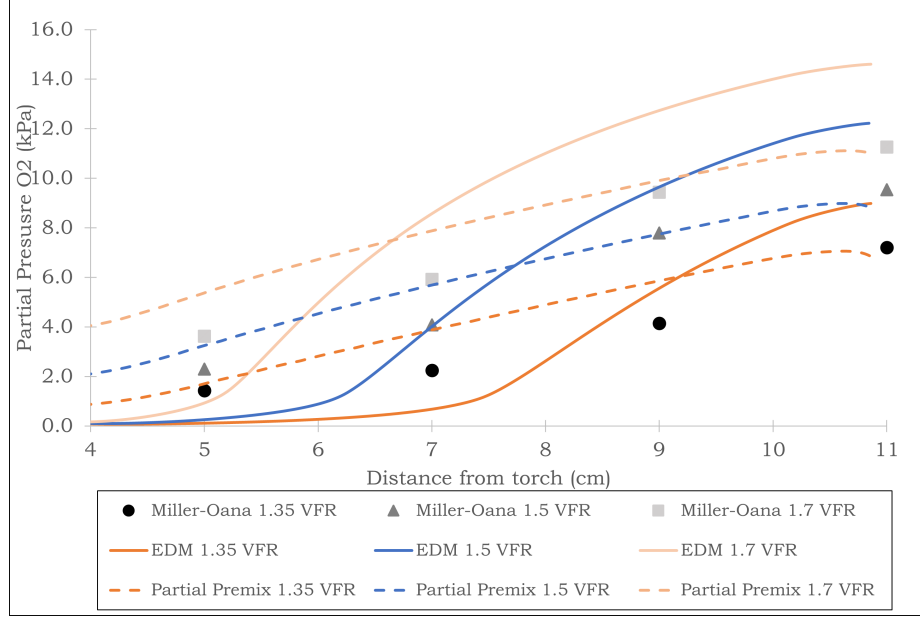


Figure 4.26: Partial pressure of O₂ at distances along the flow axis

tion affects the sample. Partial pressures were reported by Miller-Oana et al. and compared to both models in this study. To plot the partial pressures a new function using 4.2 was created in the solver and the data was exported.

$$P_{o_2} = \chi_{o_2} P_{absolute} / 1000 \quad (4.2)$$

where,

χ = mole fraction of oxygen

P = pressure

As shown in Figure 4.26, EDM overpredicts the partial pressure of oxygen at a much faster rate while the Partially Premixed model predicts a more linear rate, yet still overpredicts the partial pressure of oxygen at smaller distances to the sample.

Overall static pressures on the sample face are only slightly higher than atmospheric. At the nearest point, 5cm, pressure rises from atmospheric 101.325kPa to approximately 103.8kPa. The higher pressure, temperatures, partial pressures of O₂, and heat flux all cause the ablation and recession rates to increase. As discussed earlier in this work, to adequately model the viscous sub-layer of the boundary layer

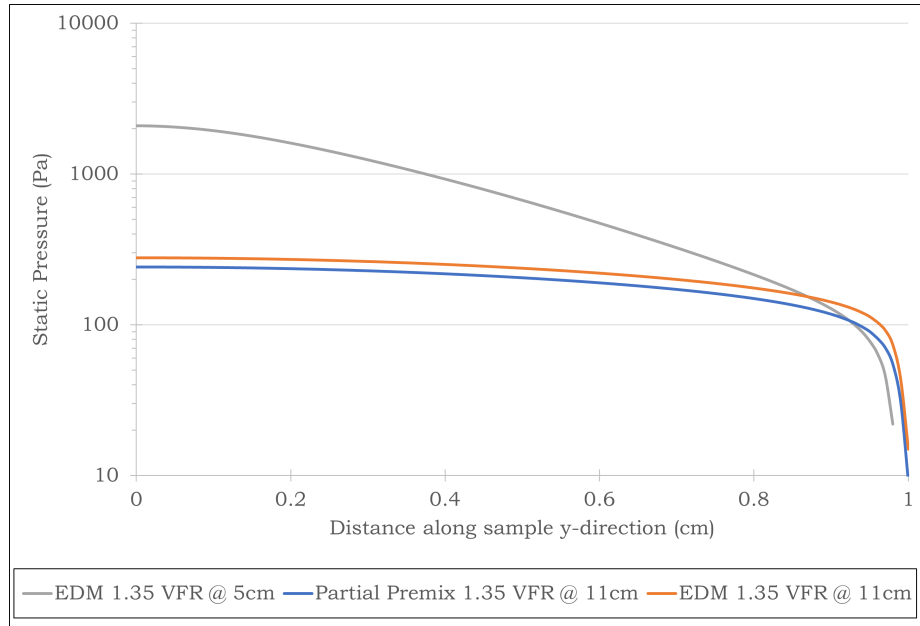


Figure 4.27: Static pressure profiles along the sample wall

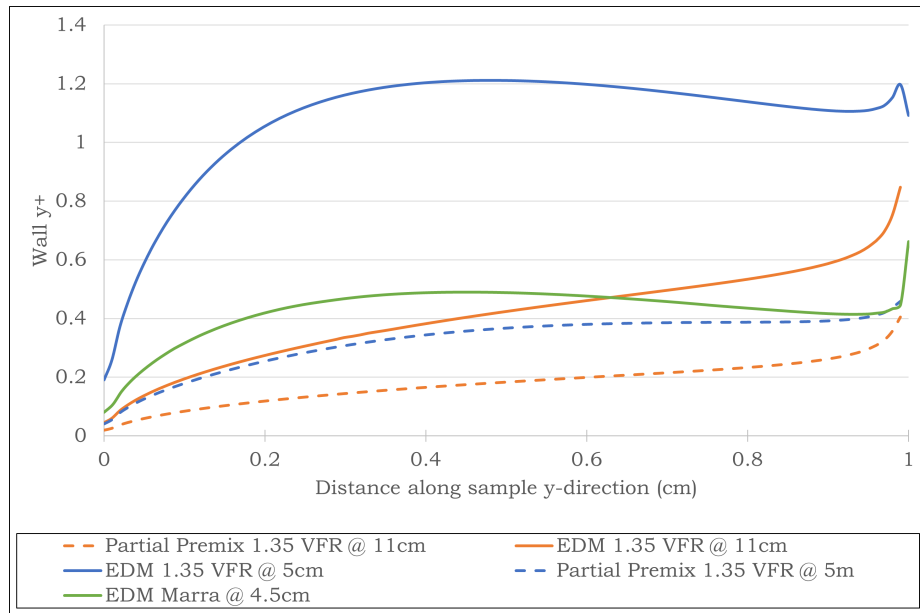


Figure 4.28: Wall y^+ profiles along the sample for EDM and Partially Premixed models at 5cm and 11 cm

the proper wall y^+ must be reached. The wall y^+ values shown in Figure 4.28 are all near unity. This shows adequate resolution of the viscous boundary layer and the thermal boundary layer allowing for accurate flow and thermal conditions along the sample. The heat transfer coefficient along the sample face was also investigated

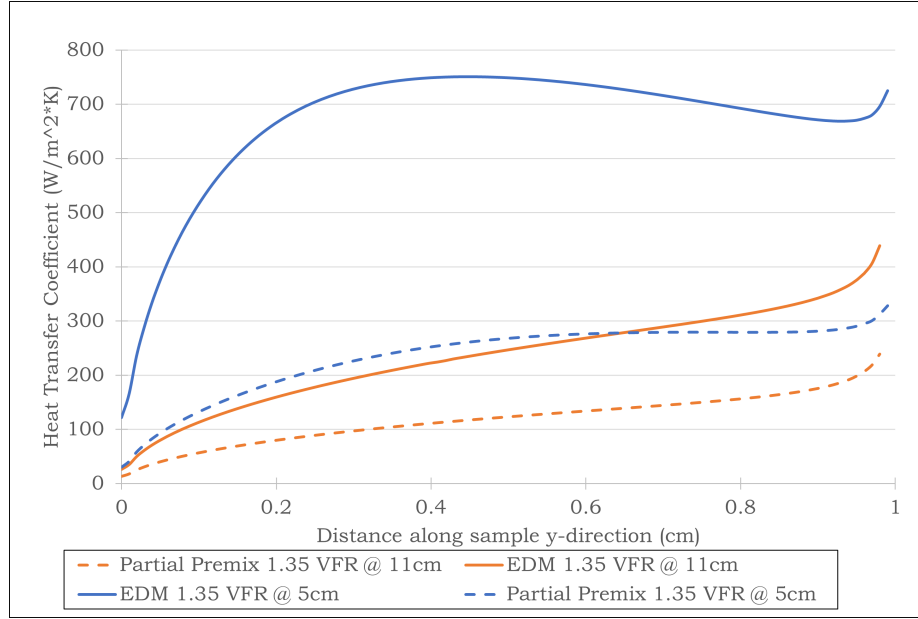


Figure 4.29: Heat transfer coefficient (y^+ based) along the sample wall

and included in Figure 4.29 for reference. The “ y^+ based heat transfer coefficient” seen in this study uses the y^+ value specified as a reference value in the setup to determine where the heat transfer coefficient is approximated. For this case, the wall y^+ was set to 100 as a reference. The surface Nusselt was found by using the reference temperature specified in the setup, shown in Figure 4.30. The reference value was changed post-solution to match the free stream combustion temperature of 4800K and 3800K, for 5cm and 11cm from the torch tip, respectively. To solve for the material response of an ablative material without a fully coupled CFD model, the uncoupled film coefficient (heat transfer coefficient method) may be used. This method uses the flow conditions that are found around an object to be used as input as boundary conditions to a material response solver. The inputs that are typically required are pressure, the boundary edge enthalpy, heat flux, and the local heat transfer coefficient which can be expressed as the Stanton Number [29],

$$htc = \frac{q}{(h_r - h_w)} = \rho_e u_e C_H \quad (4.3)$$

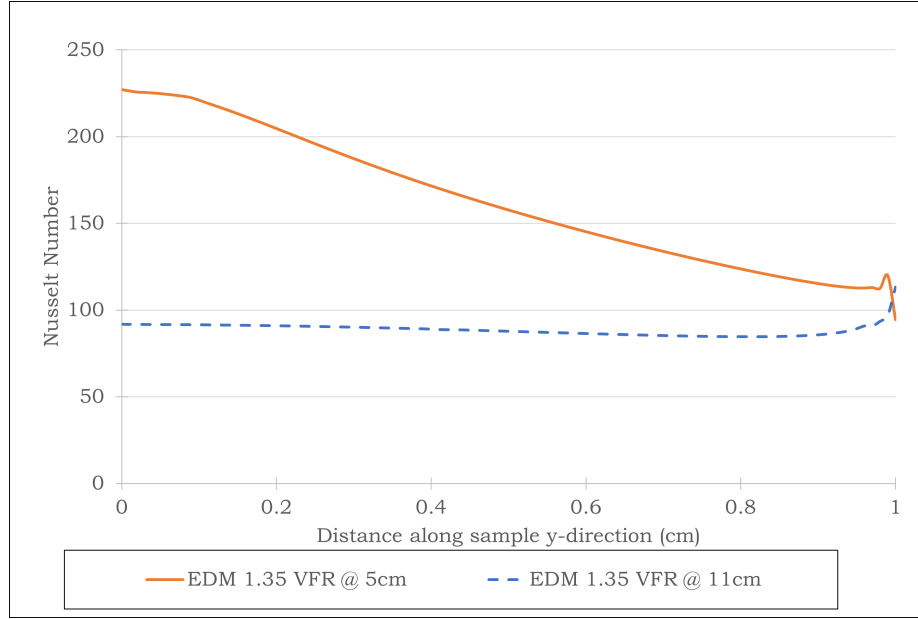


Figure 4.30: Nusselt values for the EDM with 1.35VFR at 11cm from the torch tip.

q = heat flux

h_r = recovery enthalpy

h_w = wall enthalpy

ρ_e = edge density

$St = C_H$ = Stanton Number

Flow conditions are taken at the boundary layer edge which requires knowledge of the position of the boundary layer. The boundary layer thickness was found by making the assumption of a turbulent flat plate with 3000K air flowing against it. The air kinematic viscosity was taken from Incropera et al.[41] as $8.4E-5 \text{ m}^2/\text{s}$ and an initial Reynolds number was calculated such that a turbulent boundary layer was assumed and calculated using Eq. 4.4. Then the combustion mixture properties were taken from the CFD at that point, and then the calculation was run again. Finally, a Reynolds number of $Re = 7.5E4$ was found and the thickness of the boundary layer was determined to be $\delta = 0.35\text{mm}$ based on the turbulent formula Eq. 4.4 from Incropera et al. [41]. This is in alignment with the Marra et al. approximated

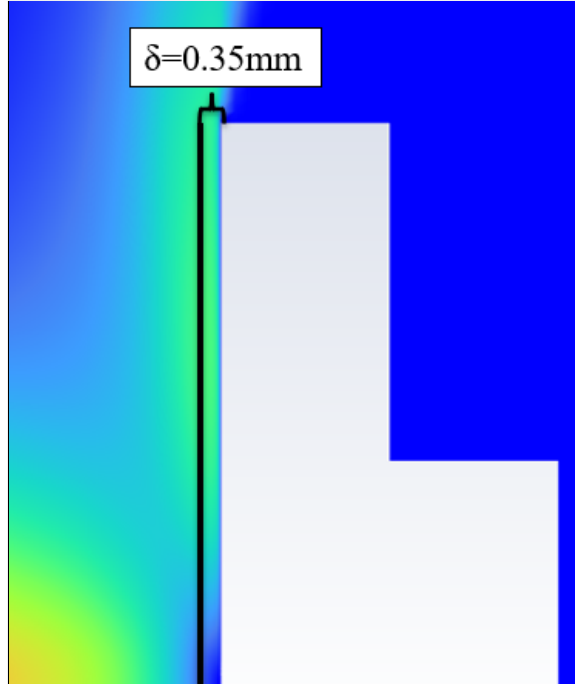


Figure 4.31: The boundary layer edge against velocity contour plot with a thickness of 0.4mm

boundary layer thickness of 0.5mm. To find the edge position along the axis the boundary layer thickness is subtracted from the sample wall distance.

$$\delta = 0.37xRe_x^{-\frac{1}{5}} \quad (4.4)$$

where,

δ = boundary layer thickness

x = distance along

Re_x = Reynolds number

As mentioned earlier, the uncoupled material response solver requires heat flux, pressure, and Stanton number as input. The Stanton number is calculated by using the CFD edge density, edge velocity, boundary edge enthalpy (h_e), the initial “cold wall” enthalpy (h_w), and heat flux. To begin solving for the Stanton number the

recovery factor and recovery enthalpy are calculated using Eq. 4.5,

$$h_r = h_e + r \frac{u_e^2}{2} \quad (4.5)$$

where,

h_r = recovery enthalpy

h_e = edge enthalpy

r = recovery factor

u_e = edge velocity

the recovery factor is often given as,

$$r = \sqrt{Pr} \text{ for laminar boundary layers}$$

$$r = \sqrt[3]{Pr} \text{ for turbulent boundary layers}$$

but is assumed unity in this work. The CFD edge enthalpy at a sample distance of 5cm is found to be $h_e = 2.46E6$ J/kg. This study does not experience flow above Mach 0.6 making the velocity component of the recovery enthalpy much less than the edge enthalpy and therefore neglected in Eq. 4.5[44][34] making recovery enthalpy equal to the boundary layer edge enthalpy.

Now that the majority of our edge conditions and CFD values have been found, the rest of the surface energy balance equations of an ablative surface may be found. The ablating wall with gas injection into the boundary layer must be solved by the use of a thermochemistry solver. Once all these variables are acquired they may be used as input into a material response solver to solve the ablation problem.

Chapter 5 Conclusions and future work

Oxyacetylene combustion is a complex phenomenon to study and model. The modeler must make several assumptions and validate the results to achieve accurate results in a timely manner. This study achieved that goal through the analysis of the Eddy-Dissipation model using relaxation to equilibrium chemistry and the Partially Premixed model.

EDM produced results with decent agreement with Miller Oana et al. for heat flux data and partial pressures of oxygen, yet it overpredicts the potential core of the jet and flame front. This over-prediction causes the flame to extend further downstream and flow values to be inaccurate. EDM is known to overestimate the flame temperature above experimental data and calculate adiabatic flame temperature values. These overestimations seem to occur at high exit velocities with small hydraulic diameters. When larger tip sizes and lower mass flow rates were used, as in the experiment done by Marra et al., EDM agrees with both experimental data and CFD data. EDM performed much faster than the EDC method used by Marra as well. The EDM method should not be discounted from use for these issues; nevertheless, it could be used when the flow is closer to, or less than, Mach 0.3.

The Partially Premixed model with non-adiabatic equilibrium achieved more accurate results when compared to the EDM cases with Miller-Oana and Marra validation cases. The partial pressures of oxygen were produced at a more linear rate and were similar to the experiment data. Flame temperatures were accurately calculated when compared to adiabatic temperatures. Velocity along the axis of flow had spikes and dips that seem odd at first; however, are accounted for by looking at the flame profile and what occurs to the temperature and density. The downside of using this model is that the temperatures cannot be fixed in the sample domain which would allow for heat flux to be validated with a cooled gauge. For ablative samples, like the one used

by Marra, the Partially Premixed model performed well. The flame temperatures that were predicted were below the CFD results of Marra and Fortner but more accurate because Eddy-Dissipation models over predict the temperature. Therefore, the Partially Premixed model would perform best when oxyacetylene experiments have slower flow velocities, for a wide range of equivalence ratios. This model accurately predicts boundary layer edge properties and thickness which can be used in material response solvers, such as the Kentucky AeroThermal Solver (KATS).

5.1 Future work

Though the Partially Premixed model aligns very well with experimental data and is computationally efficient, it lacks validation against heat flux values. More modeling is needed with non-isothermal samples to validate the Partially Premixed model. The use of user-defined functions also needs to be investigated attempt to “trick” the solver in to behaving as an isothermal sample at every iteration.

The Eddy-Dissipation Concept solver could be investigated to account for higher velocity flows where density changes are large, and the Damköhler number approaches unity. This model would take into account the chemical kinetics of the reactions and could yield better results. The equilibrium method may aid in faster convergence if used as initial values for the EDC model. Mesh motion in Fluent™ was left for future work and would allow the coupling of the CFD solver to a material response solver.

A main goal for future research would be to use the well-predicted solutions in this work to solve for ablation using the film coefficient method in the Kentucky AeroThermal Solver or similar material response solvers. Ablative rates could be compared to Marra et al. along with other works when completed.

Appendices

Appendix A Partial Pressure custom function

The solver does not have a built-in variable for the partial pressure of a species, therefore one is created. The variable is created by way of a custom function that is equal to Eq.4.2.

```
(custom-field-function/define
  '((
    (name pp-o2) (display "olef-o2 * absolute-pressure / 1000")
    (syntax-tree ("/" ("*" "molef-o2" "absolute-pressure") 1000))
    (code (field-/ (field-* (field-load "molef-o2")
      (field-load "absolute-pressure"))) 1000))
  ))
)
```

Appendix B Automatic initialization commands (Cold Flow)

This command is used during automatic initialization and ensures that the reactions are turned off and then we patch the domain with oxygen.

```
/define/models/species/volumetric-reactions n  
/solve/patch fluid.1 () () species-1 n 0.23
```


Appendix C Automatic initialization commands (Combustion)

This command is used during automatic initialization and initiates combustion. The reactions are first turned on, products are patched into the ignition area, and then the solver is run.

```
/define/models/species/volumetric-reactions y  
/solve patch () 0 () species-2 n 0.1  
/solve patch () 0 () species-3 n 0.1  
/solve/set/pseudo-time-method/global-time-step-settings y 1 0.01 y 0.1
```

Appendix D Custom Ablative Material

Using the table and values specified by Marra et al. [1] a custom material was created. The specific heat and thermal conductivity are defined by a piecewise linear polynomial.

```
((sigratherm solid
  (chemical-formula . #f)
  (density (constant . 445.))
  (specific-heat (
    polynomial piecewise-linear (300. . 700.)
    (673. . 1480.) (1073. . 1840.)
    (1873. . 2060.) (2173. . 2100.))
  (thermal-conductivity (
    polynomial piecewise-linear (300. . 0.17)
    (673. . 0.32) (1073. . 1.07)
    (1873. . 2.6) (2173. . 3.7))
  (molecular-weight (constant . 76.94))
  (struct-youngs-modulus (constant . 100000000.))
  (struct-poisson-ratio (constant . 0.2))
  (absorption-coefficient (constant . 0.))
  (scattering-coefficient (constant . 0.))
  (scattering-phase-function (isotropic . #f))
  (refractive-index (constant . 1.))
  ))
```

Bibliography

- [1] Marra, F., Pulci, G., Tirilló, J., Bartuli, C., and Valente, T., “Numerical Simulation of Oxy-Acetylene Testing Procedure of Ablative Materials for Re-Entry Space Vehicles,” *Proceedings of the Institution of Mechanical Engineers, Part L: Journal of Materials: Design and Applications*, Vol. 225, 2011. doi:10.1177/14644207JMDA335.
- [2] Fortner, L., “Numerical Investigation of an Oxyacetylene Torch With Regards to an Ablative Material,” Master’s thesis, University of Kentucky, 2022. doi:10.13023/ETD.2022.026.
- [3] Miller-Oana, M., Neff, P., Valdez, M., Powell, A., Packard, M., Walker, L. S., and Corral, E. L., “Oxidation Behavior of Aerospace Materials in High Enthalpy Flows Using an Oxyacetylene Torch Facility,” *Journal of the American Ceramic Society*, Vol. 98, 2015. doi:10.1111/jace.13462.
- [4] Glassman, I., *Combustion*, 2nd ed., Academic Press, San Diego New York Boston [etc.], 1987.
- [5] Strehlow, R. A., *Combustion fundamentals*, McGraw-Hill series in energy, combustion, and environment, McGraw-Hill, New York, 1984.
- [6] Zuckerman, N., and Lior, N., “Impingement Heat Transfer: Correlations and Numerical Modeling,” *Journal of Heat Transfer*, Vol. 127, 2005. doi:10.1115/1.1861921.
- [7] van der Meer, T. H., “Heat transfer from impinging flame jets,” Ph.D. thesis, Delft University, Netherland, Sep. 1987.
- [8] ASTM, “Test Method for Oxyacetylene Ablation Testing of Thermal Insulation Materials,” Tech. rep., ASTM International, 2020. doi:10.1520/E0285-08R20.

- [9] Baukal, C. E., *Oxygen-Enhanced Combustion*, 2nd ed., CRC Press, Hoboken, 2013.
- [10] Magnussen, B., and Hjertager, B., “On mathematical modeling of turbulent combustion with special emphasis on soot formation and combustion,” *Symposium (International) on Combustion*, Vol. 16, 1977. doi:10.1016/S0082-0784(77)80366-4.
- [11] Oran, E. S., and Boris, J. P., *Numerical approaches to combustion modeling*, Progress in astronautics and aeronautics ; v. 135, American Institute of Aeronautics and Astronautics, Washington, DC, 1991.
- [12] Yusuf, U., Masud, J., Zia, U., Sher, I., Zakir, J., and Siddiqui, M., “Modelling of Supersonic Combustion using Finite-Rate Eddy-Dissipation (FRED) and Eddy-Dissipation Concept (EDC) Turbulence Chemistry Interaction (TCI) Models,” *AIAA SCITECH 2023 Forum*, AIAA SciTech Forum, American Institute of Aeronautics and Astronautics, 2023. doi:10.2514/6.2023-1689.
- [13] Hoste, J.-J. O., “Scramjet combustion modeling using eddy dissipation model,” Ph.D. thesis, University of Strathclyde, 2018. doi:10.48730/JMAG-CD95.
- [14] Crawford, B., Verma, I., Orsino, S., Cagnone, J., and Li, S., “Validation of the new modeling capabilities of the Ansys Fluent CFD high-speed solver for the simulation of supersonic combustion in Scramjets and Rotating Detonation Engines,” .
- [15] Zeldovick, Y., “On the Theory of Combustion of Initially Unmixed Gases,” *NACA Technical Memorandum 1296*, 1949.
- [16] Bilger, R. W., “Turbulent flows with nonpremixed reactants,” *Turbulent Reacting Flows*, edited by P. A. Libby and F. A. Williams, Topics in Applied Physics, Springer, Berlin, Heidelberg, 1980. doi:10.1007/3540101926_9.

- [17] Baukal, C. E., Gershtein, V. Y., and Li, X., *Computational fluid dynamics in industrial combustion*, Industrial combustion series, CRC Press, Boca Raton, FL, 2001.
- [18] Inc., A., “ANSYS Fluent Theory Guide 2023R2,” , 2023.
- [19] Bray, K. N. C., “Turbulent flows with premixed reactants,” *Turbulent Reacting Flows*, edited by P. A. Libby and F. A. Williams, Topics in Applied Physics, Springer, Berlin, Heidelberg, 1980. doi:10.1007/3540101926_10.
- [20] Zimont, V., and Lipatnikov, A., “A numerical model of premixed turbulent combustion of gases,” *Chemical Physics Reports*, Vol. 14, 1995, pp. 993–1025.
- [21] Zimont, V., Polifke, W., Bettelini, M., and Weisenstein, W., “An Efficient Computational Model for Premixed Turbulent Combustion at High Reynolds Numbers Based on a Turbulent Flame Speed Closure,” *J. Eng. Gas Turbines Power*, 1997.
- [22] Aydin, M., “Characterization of an Acetylene-Oxygen Flame for Material Studies on High-Temperature Materials,” Ph.D. thesis, Ruhr University Bochum, 2020.
- [23] Snyder, C., “Chemical Equilibrium with Applications Online,” , 2018. URL <https://cearun.grc.nasa.gov/>.
- [24] Westbrook, C. K., and Dryer, F. L., “Simplified Reaction Mechanisms for the Oxidation of Hydrocarbon Fuels in Flames,” *Combustion Science and Technology*, Vol. 27, No. 1-2, 1981, pp. 31–43. doi:10.1080/00102208108946970.
- [25] Crawford, D. H., and McCauley, W. D., “Investigation of the Laminar Aerodynamic Heat-Transfer Characteristics of a Hemisphere-Cylinder in the Lngely 11-inche Hypersonic Tunnel at a Mach Number of 6.8,” *NACA Technical Note 3706*, 1956.

- [26] Sibulkin, M., “Heat Transfer Near the Forward Stagnation Point of a Body of Revolution,” *Journal of Aerospace Science*, Vol. 19, No. 8, 1952, pp. 570–571.
- [27] Fay, J. A., and Riddell, F. R., “Theory of Stagnation Point Heat Transfer in Dissociated Air,” *Journal of the Aerospace Sciences*, Vol. 25, No. 2, 1958, pp. 73–85. doi:10.2514/8.7517, publisher: American Institute of Aeronautics and Astronautics.
- [28] Cooper, J., “A Decoupled Engineering Methodology for Accurate Prediction of Ablative Surface Boundary Conditions in Thermal Protection Systems,” Ph.D. thesis, University of Kentucky Libraries, 2022. doi:10.13023/ETD.2022.131.
- [29] Bianchi, D., “Modeling of ablation phenomena in space applications,” Ph.D. thesis, University of Rome La Sapienza, 2007.
- [30] Amar, A. J., Oliver, B., Kirk, B., Salazar, G., and Droba, J., “Overview of the CHarring Ablator Response (CHAR) Code,” doi:10.2514/6.2016-3385.
- [31] Wright, M. J., Candler, G. V., and Bose, D., “Data-Parallel Line Relaxation Method for the Navier-Stokes Equations,” *AIAA Journal*, Vol. 36, No. 9, 1998, pp. 1603–1609. doi:10.2514/2.586.
- [32] Menter, F. R., “Two-equation eddy-viscosity turbulence models for engineering applications,” *AIAA Journal*, Vol. 32, No. 8, 1994, pp. 1598–1605. doi:10.2514/3.12149.
- [33] Inc., A., “ANSYS Fluent User’s Guide 2023R2,” , 2023.
- [34] Anderson, J., *Hypersonic and High Temperature Gas Dynamics*, American Institute of Aeronautics and Astronautics, Reston, UNITED STATES, 2000.
- [35] Ren, Z., and Goldin, G. M., “An efficient time scale model with tabulation of chemical equilibrium,” *Combustion and Flame*, Vol. 158, No. 10, 2011, pp. 1977–1979. doi:10.1016/j.combustflame.2011.02.018.

- [36] Ren, Z., Goldin, G. M., Hiremath, V., and Pope, S. B., “Simulations of a turbulent non-premixed flame using combined dimension reduction and tabulation for combustion chemistry,” *Fuel*, Vol. 105, 2013, pp. 636–644. doi:10.1016/j.fuel.2012.08.018.
- [37] Emami, S., Jafari, H., and Mahmoudi, Y., “Effects of Combustion Model and Chemical Kinetics in Numerical Modeling of Hydrogen-Fueled Dual-Stage HVOF System,” *Journal of Thermal Spray Technology*, Vol. 28, No. 3, 2019. doi:10.1007/s11666-019-00826-8.
- [38] Borman, G. L., and Ragland, K. W., *Combustion engineering*, McGraw-Hill, Boston, 1998.
- [39] Turns, S. R., *An introduction to combustion: concepts and applications*, McGraw-Hill series in mechanical engineering, McGraw-Hill, New York, 1996.
- [40] Keating, E. L., *Applied combustion*, No. 79 in Mechanical engineering, M. Dekker, New York, 1993.
- [41] Incropera, F. P., and Incropera, F. P. (eds.), *Fundamentals of heat and mass transfer*, 6th ed., John Wiley, Hoboken, NJ, 2007. OCLC: ocm62532755.
- [42] White, K., “Welding Tip Chart,” , 2010. URL <https://www.tinmantech.com/products/welding/meco-torch-accessories/welding-tip-chart.php>.
- [43] Pope, S., “Computationally efficient implementation of combustion chemistry using in situ adaptive tabulation,” *Combustion Theory and Modelling*, Vol. 1, No. 1, 1997, pp. 41–63. doi:10.1080/713665229.
- [44] Bertin, J. J., *Hypersonic aerothermodynamics*, AIAA education series, American Institute of Aeronautics and Astronautics, Washington, DC, 1994.

Vita

Craig Meade is a Kentucky native who graduated from the University of Kentucky with a Bachelor of Science in Mechanical Engineering. While at university he was placed on the Dean's List and received the A.S.M.E. Petroleum Division scholarship. He has worked for 10 years in the natural gas industry for Louisville Gas & Electric, Louisville Kentucky. During this time he obtained his Professional Engineer license in 2019. Current research interests include fracture mechanics, material response, and CFD.